Contents — H through K

THE LOCH LEVEN CRATER: ANATOMY OF A LOW-ANGLE OBLIQUE IMPACT STRUCTURE.

B. J. Hamill, Wester Tillyrie House, Milnathort, Kinross, Scotland KY13 0RW. b.hamill@zoo.co.uk

Synopsis: The Loch Leven basin (56° 12' N, 3° 23' W) in the Midland Valley of Scotland has been identified as the site of the primary impact of a low-angle oblique impact event dating from the end of the Carboniferous. Together with two further downrange structures, it forms a chain of craters which appear to have been produced by fragments of a large asteroid which disintegrated on impact.

Topography: The Loch Leven crater of Kinross-shire, East-Central Scotland is an elongated structure (18 x 8 km) which lies 30 km N of Edinburgh and 40 km SW of St. Andrews (Fig. 1). It has been preserved by a quartz-dolerite sill which was emplaced around the edges of the crater infill and dates from 290 Ma. The sill was intruded at a depth of 1.8 km, so that the structure which survives represents the eroded base of the crater. The structure has a central ridge and a series of lateral terraces (Fig 2). By analogy with the features of the lunar crater Schiller [1] and other elliptical craters [2], Loch Leven is believed to be a low-angle oblique impact structure. These structures result from impact of objects which disintegrate into multiple fragments before burial. The fragments ricochet downrange, forming multiple secondary impact structures [2].

Petrology: Impactites of the structure include impact melts, suevites, lithic breccias and friction-melt rocks. The country rocks of the Loch Leven area are mostly lower Carboniferous sandstones and some of these have been affected by the impact. At the eastern (proximal) end of the structure, thermal effects dominate, with formation of indurated quartzitic rocks containing tridymite (Fig 3, SEM) and devitrified glassy textures (Fig 4, XPL) but no Planar deformation features (PDFs). At the western (distal) end of the structure, however, target rocks do contain PDFs (Fig 5, XPL), supporting previous theoretical predictions of an asymmetric "canoe-shaped" distribution of shock pressures in these oblique structures [1]. Interstitial melting textures are common in these rocks, and new-growth micas are seen between grain boundaries in otherwise "normal" sandstones (Fig 6, SEM).

The most altered lithologies are found in the central ridge of the structure which contains some highly vesicular rocks one of which is mainly composed of vesiculated lechatelierite (Fig 7, SEM). Unaltered quartz grains in this rock contain planar fractures and PDFs (Fig 8, oil mount, XPL).

The structure also contains a distinctive suite of pale flow-banded glassy rocks which are interpreted as friction melts. These are preserved along the southern rim of the crater and are believed to be the product of melting of a mixture of asteroid material and sedimentary target rocks. The rocks contain altered glassy pyroxenes in a flow-banded quartzo-feldpathic matrix (Fig 9) which shows a distinctive laminated devitrification texture (Fig 10, XPL).

Suevites (Fig 11) are found in many places in the crater and contain abundant felsic clasts in which feldspar phenocrysts display a "checkerboard" texture (Fig 12, XPL).

There are numerous outcrops of basalt in the northern and western parts of the structure. These are believed to represent the remains of melt-sheets of the crater floor. Basalts of the central ridge include composite rocks in which a macroporphyritic and microporphyritic component are present simultaneously and behave as immiscible liquids (Fig 13). This phenomenon has been reported in "Tagamites" of the Popigai structure [3].

References: [1] Melosh, H. J. (1989), *Impact Cratering* (OUP). [2] Schultz, P.H. & Gault, D.E. (1990), *GSA Spec. Pap. 247*, 239-261. [3] Masaitis, V.L. (1994), *GSA Spec. Pap. 293*, 153-162.

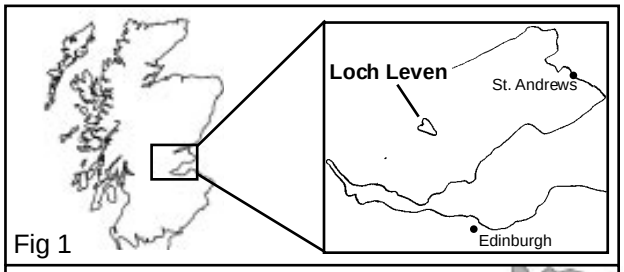

Fig 1

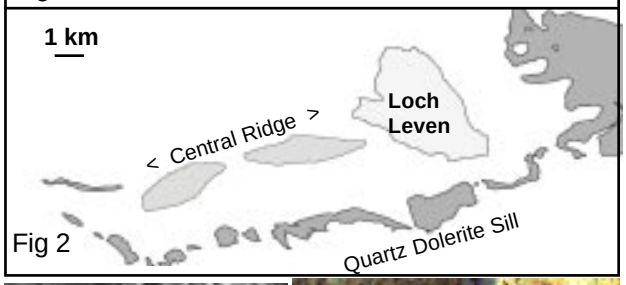

Fig 2

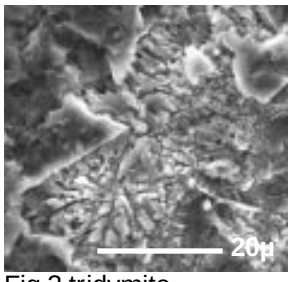

Fig 3 tridymite

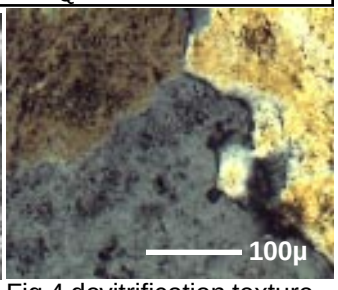

Fig 4 devitrification texture

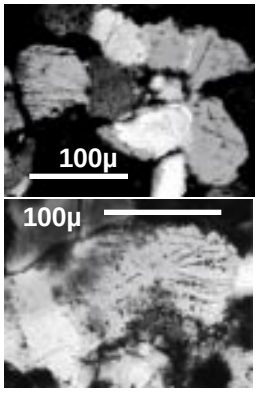

Fig 5 PDFs

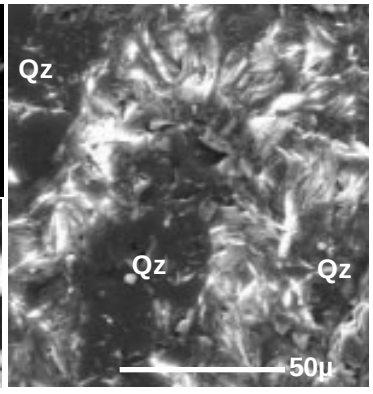

Fig 6 interstitial mica growth

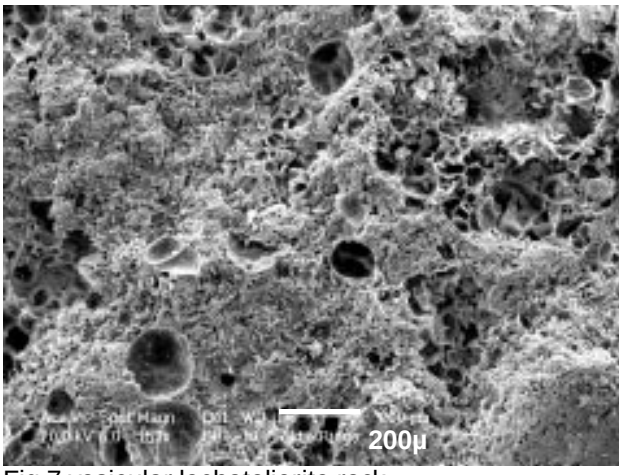

Fig 7 vesicular lechatelierite rock

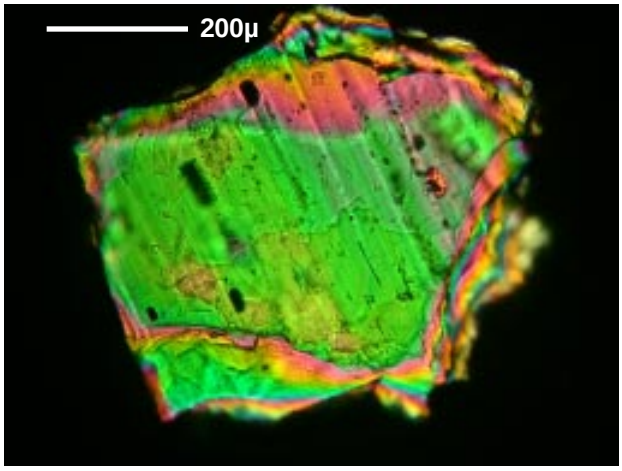

Fig 8 PDFS in quartz grain

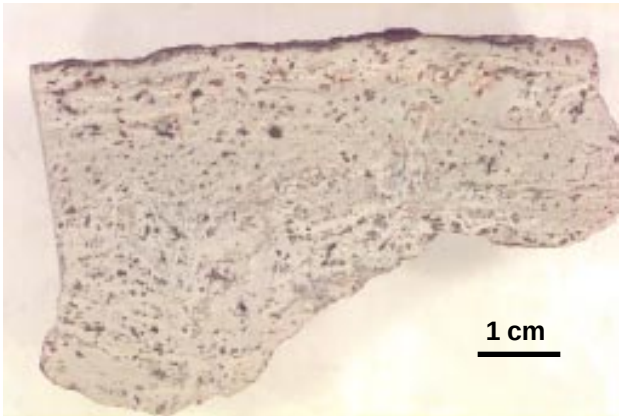

Fig 9 flow-banded friction-melt rock

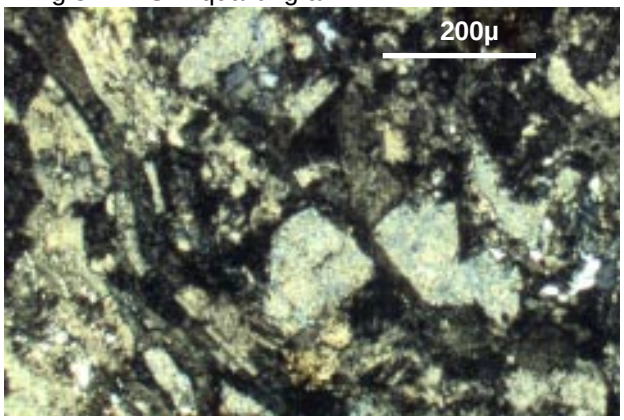

Fig 10 laminated devitrification texture

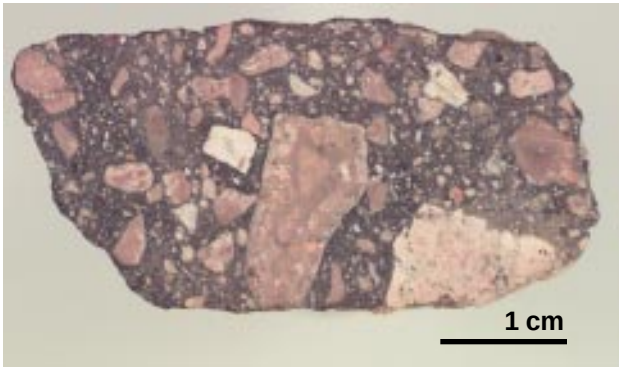

Fig 11 suevite

Fig 12 checkerboard texture in feldspar

Fig 13 Composite melt-rock ("Tagamite?") showing a macroporphyritic and microporphyritic component present simultaneously, and behaving as immiscible liquids

A TRIPLE COMPLEX OF LOW-ANGLE OBLIQUE IMPACT STRUCTURES IN THE MIDLAND VALLEY OF SCOTLAND. B. J. Hamill, Wester Tillyrie House, Milnathort, Kinross, Scotland KY13 0RW. b.hamill@zoo.co.uk

Synopsis: A linear chain of three elliptical impact structures has been identified in the Midland Valley of Scotland. These structures appear to have been produced by fragments of a large asteroid which disintegrated on impact. The primary impact site was the Loch Leven basin (56° 12' N, 3° 23' W), which is an elongated structure (18 x 8 km) with a central ridge and lateral terraces. Field evidence suggests an end-Carboniferous date for this impact, similar to that of several known North American craters and suggesting that this was a global event which may have been implicated in the disappearance of the forests of Laurentia and Laurussia.

Field evidence: The Loch Leven basin of Kinrossshire, east-central Scotland lies 30 km N of Edinburgh and 40 km SW of St. Andrews. It is an elliptical low-lying area surrounded on three sides by quartz-dolerite hills of the Midland Valley Sill (290 Ma), which appears to have been intruded around the edges of the debris infill of the crater, thereby preserving its shape. The sill is known to have been intruded at depth (1.8 km), and the present-day structure therefore represents only the eroded base of the crater. Vestigial outcrops of impactites are preserved close to the quartz-dolerite and include impact melts, suevites, lithic breccias and friction-melt rocks. The structure also has a central ridge composed of basalts and basaltic breccias, which hosts the most altered rocks, including highly vesiculated "frothed" clasts in breccias. A series of lateral terraces runs parallel to this ridge. These features are also seen in the lunar crater Schiller, which is believed to be a low-angle oblique impact structure [1]. Such structures are formed under rare circumstances in which the impactor is not effectively buried but instead disintegrates into multiple fragments which ricochet downrange and form secondary impacts elsewhere [2].

A second structure downrange of Loch Leven is indicated by a semi-circular arrangement of rock outcrops centered near Bannockburn, Stirlingshire, 30 km WSW of Loch Leven. This structure is composed of coarse breccias and melt rocks, and a natural cross-section through what is believed to be the north wall of the crater is exposed along the line of the Ochil fault. As at Loch Leven, the shape of the structure is partially preserved by peripheral quartz-dolerite intrusions of the Midland Valley Sill.

A third downrange structure is represented by the plateau of the Gargunnock Hills W of Stirling, an elliptical area (14 x 6 km) of basalts previously interpreted as of volcanic origin. Field evidence demonstrates the existence of two separate series of basalts in which the upper series is overprinted on the lower series and also forms low-angle intrusions into both the volcanic rocks and sedimentary rocks of known stratigraphic position. A distinctive lithology in these rocks (the Kirkwood formation), previously interpreted as a detrital sedimentary rock because of its intense stratification, probably represents a transitional "buffer zone" facies between the static country rocks and a high-velocity body of intrusive melt-rock. It shows laminar flow properties, demonstrating the existence of a velocity gradient across the interface between sub-horizontally intruded impact melts and the target rocks. The Gargunnock structure is believed to represent the eroded base of a crater floored by impact melts. The crater walls have been removed by erosion and the floor survives as a pedestal crater. The Kirkwood formation is widespread in western Scotland and there may therefore be several further impact structures in the area.

Petrologic data:

Loch Leven structure. A variety of impact effects are observed in the Loch Leven structure, in which the country rocks are mostly sandstones. At the eastern (proximal) end of the structure, thermal effects dominate, with formation of indurated quartzitic rocks containing tridymite and devitrified glasses but no Planar deformation features (PDFs). At the western (distal) end of the structure, target rocks do contain PDFs (Fig 1, PPL) and planar fractures (Fig 2, XPL) and the presence of residual glass in these features is confirmed by SEM of HF-etched grains from these sandstones (Fig 3).

The most altered lithologies are found in the central ridge of the structure which contains many vesiculated rocks. One highly "frothed" clast is largely composed of grains of vesicular lechatelierite (Fig 4, SEM) and the unvesiculated quartz cores of these grains are revealed by HF treatment (Fig 5). Unaltered grains of quartz in this rock commonly have a tabular habit produced by a set of basal planar fractures and also contain PDFs (Fig 6, oil mount).

The structure also contains a distinctive suite of pale flow-banded glassy rocks which are interpreted as friction melts.

Bannockburn structure. A coarse immature sandstone from the central part of the structure contains PDFs in quartz and feldspar and is believed to be a "wash-back" impact breccia. PDFs are also found in clasts of coarse breccias on the north wall of the structure and in the underlying country rocks.

Gargunnock structure. This structure adjoins the Bannockburn structure and PDFs found in the underlying country rocks are therefore ambiguous. No PDFs have yet been found in rocks uniquely associated with the

Gargunnock structure. However, basalts from the structure include composite rocks in which a macroporphyritic and microporphyritic component are present simultaneously and behave as immiscible liquids. This phenomenon has been reported in "Tagamites" of the Popigai structure [3]. Similar rocks are present at Loch Leven.

Global implications: An end-Carboniferous date for the impact event is suggested by the field relationships with the Midland Valley Sill and supported by anomalous K-Ar dates obtained for some of the Gargunnock hills basalts [4]. The sudden disappearance of the forests of Laurentia and Laurussia at the end of the Carboniferous has been attributed to climate change. However, coal-producing forests thrived throughout the Permian in China and Siberia, which were separated from the main Pangean continent at the time [5].

Analysis of known impact structures [6] shows that three small North American craters (Decaturville, Des Plaines and Ile Rouleau) of approximately end-Carboniferous date lie (within 1.3 km) on a great circle, suggesting a common provenance. A further 8 North American craters have similar ages. These could be further secondary impact craters produced by fragments of the Loch Leven asteroid, and the impacts may have contributed to the destruction of the forests.

References: [1] Melosh, H. J. (1989), *Impact Cratering*, 25 (OUP). [2] Schultz, P.H. & Gault, D.E. (1990), *GSA Spec. Pap. 247*, 239-261. [3] Masaitis, V.L. (1994), *GSA Spec. Pap. 293*, 153-162. [4] De Souza, H. (1979) Ph.D. thesis, Edinburgh. [5] Ziegler, A.M. et al., *in* Martini, I.P. (ed) *Late Glacial and Post-Glacial Environmental Changes* (1996), 111-146 (OUP). [6] Grieve, R.A.F. et al. (1995), *GSA Today 5*, 189-196.

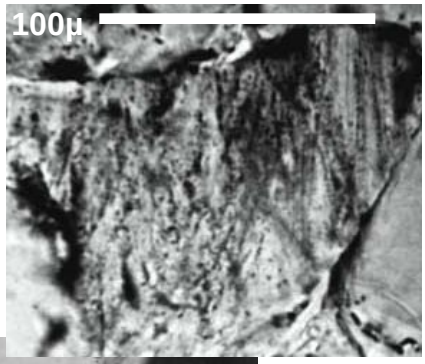

Fig 1
PDFs in
sandstone

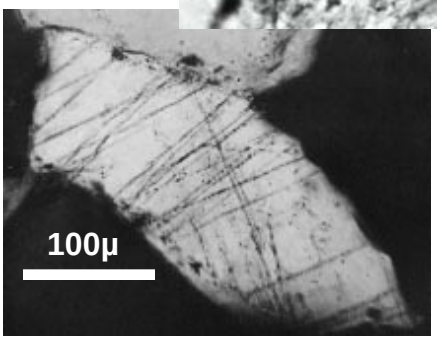

Fig 2
PDFs and
PFs in
sandstone

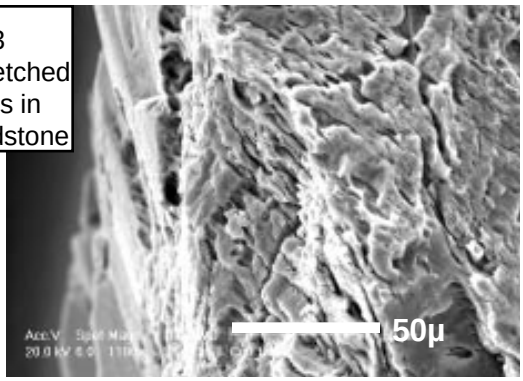

Fig 3
HF-etched
PDFs in
sandstone

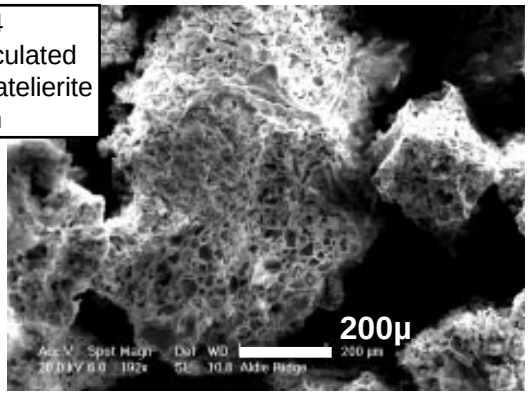

Fig 4
vesiculated
lechatelierite
grain

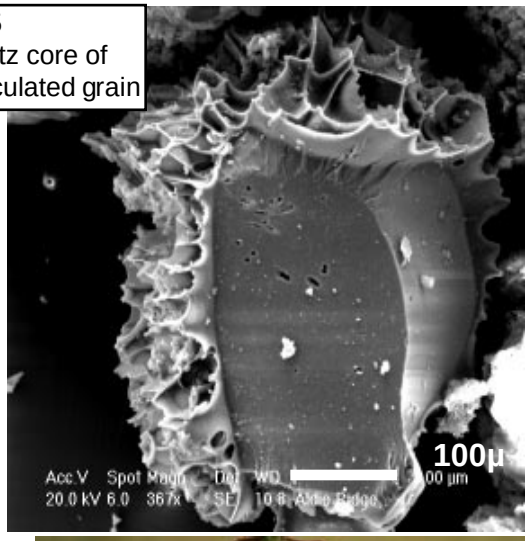

Fig 5
quartz core of
vesiculated grain

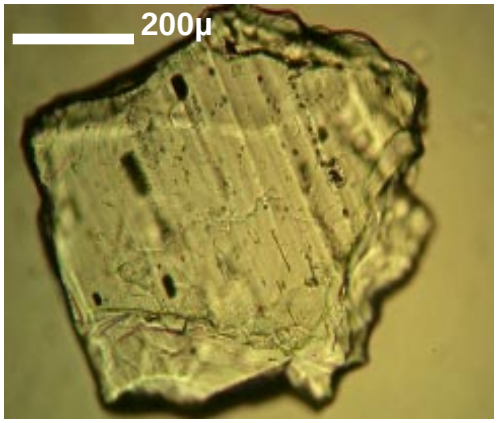

Fig 6
quartz
grain
with
PDFs

SOME RING-LIKE MAGNETIC ANOMALIES IN IMPACT STRUCTURES AND THEIR POSSIBLE CAUSES. P. J. Hawke[1], [1]School of Earth and Geographical Sciences, University of Western Australia, 35 Stirling Hwy, Crawley, 6009, Australia, phawke@ geol.uwa.edu.au.

Introduction: While not diagnostic of meteorite impact when used in isolation, geophysics is responsible for the initial discovery of many concealed craters. Airborne magnetics is one of the cheapest, and hence most widely available, of all the geophysical techniques.

Based primarily on studies of craters formed in crystalline rocks, the definitive papers on the geophysical signatures of impact craters [1],[2] suggest the main effect of extraterrestrial impact is to reduce the magnetic susceptibility of the target rock, resulting in an overall magnetic low or subdued zone. Local magnetic highs may be present, usually near the centre of complex structures. These are attributed to near surface magnetic basement within the central uplift of large structures or to shock, thermal and chemical processes forming new magnetic minerals or resetting magnetic remanence within the target rock or impact melt material. There are only a few case studies in the literature of magnetic surveys over true sedimentary targets, eg Mjølnir [3] and the sources of the observed magnetic anomalies are not well understood.

Circular magnetic anomalies: Three examples of ring-like anomalies identified in high-resolution magnetic surveys over impact structures formed in Australian sedimentary basins are presented here. A residual magnetic image for each structure is shown in Fig. 1, created by removing a second order polynomial trend from the total magnetic intensity.

The 12 km diameter Yallalie structure (30°27'S, 115°46'E) is formed in the Mesozoic sediments of the Perth Basin. While it is considered to be of possible impact origin due to the absense of shock metamorphic features, the geophysical data in [4] provide a convincing argument for its impact origin. An image of the magnetic data (Fig. 1a), collected at a 200 m line spacing and 60 m flying height, shows five concentric magnetic anomalies, centred on a single peak. These anomalies closely correlate with faults interpreted from seismic data to bound the central uplift and form terraces. The magnitude of the anomalies range between 4 and 12 nT.

The Foelsche structure (16°40'S, 136°47'E) is a partially concealed, 6 km diameter Proterozoic structure formed in the sedimentary and volcanic intrusive rocks of the McArthur Basin [5]. The structure was first recognised from magnetic data collected at a 500 m line spacing and 100 m flying height (Fig. 1b). The two concentric circular anomalies, with amplitudes of about 50 nT correlate with the outer extent of the central uplift and the crater rim.

Wolfe Creek (19°10'S, 127°48'E) is a small (880 m), young (300ka) crater formed in Devonian sandstone of the Canning Basin [6]. Magnetic data were collected at a very high resolution, 50 m line spacing and a 40 m flying height. This identified two roughly circular magnetic anomalies, coincident with the top and base of the crater wall, centred on a single peak (Fig. 1c). The amplitude of these anomalies is less than 4 nT.

Possible causes: Four possible causes of circular magnetic anomalies within impact structures are proposed. Melt rock generated by the impact is likely to form lenses of melt-fragment breccia (suevite) within the allochthonous breccia deposited on the complex crater floor and can be injected into floor as breccia dykes (Fig. 2a). Such material can carry a high magnetic remanance that is set at the time of impact. Local hydrothermal systems lasting several 10ka can be driven by the heat transferred to the target during the impact event, eg Haughton [7]. This may result in the production of new magnetic minerals from iron sources (pyrite, biotite, glauconite) within the otherwise non-magnetic sedimentary rock. Deeper magnetic sources concentrated along internal faults within the structure are expected to result from this process (Fig. 2b). A remanantly magnetised impact melt or post-impact hydrothermal activity are the most likely causes of the anomalies associated with the Mjølnir and Yallalie structures. A perfectly flat-lying magnetic unit, such as a dolerite sill, will not produce an anomaly that can be detected by a magnetic survey. Deformation of the target rock by the impact will change the dip and create truncations within this magnetic horizon (Fig. 2c) to produce magnetic edges that can be detected. A dolerite sill deformed in this manner is probably the cause of the circular magnetic anomalies observed at Foelsche. Finally, magnetic material may be deposited into the crater by normal sedimentary process after the impact event (Fig. 2d). While the magnetic response of Wolfe Creek can be partially explained by the drape of the survey, maghemite concentrated in the sandy post-impact fill by wind swirling around the crater floor is interpreted as the source of the magnetic anomaly coincident with the base of the rim wall at Wolfe Creek.

References:

[1] Henkel H. (1992) *Tectonophysics, 216,* 63-89. [2] Grieve R. A. F. and Pilkington M. (1996) *AGSO J. Aust. Geol. Geophys., 16,* 399-420. [3] Tsikalas et al. (1998) *Tectonophysics,289,* 257-280. [4] Dentith et al. (1999) *Geological Mag.,* 136, 619-632. [5] Haines P. W. and Rawlings D. J. (2002) *Meteorit. Planet. Sci. 37,* 269-280. [6] Hawke P. J. (2003) *Geological Survey of Western Australia Record 2003/10*. [7] Osinski et al. (1998) *Meteorit. Planet. Sci. 36,* 731-745.

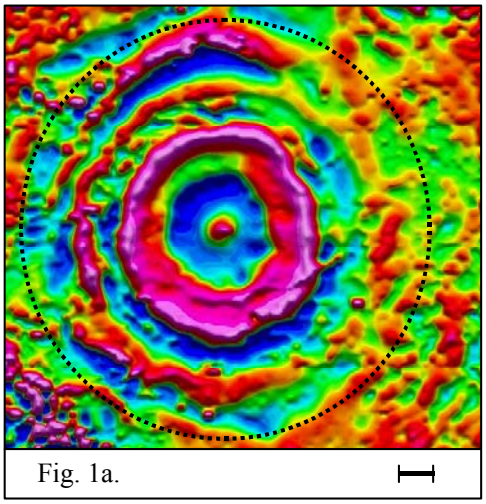

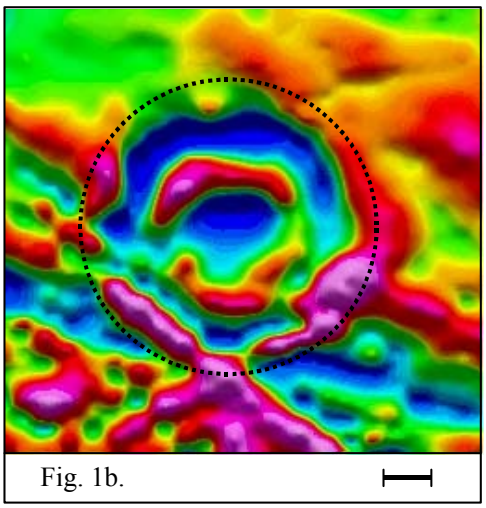

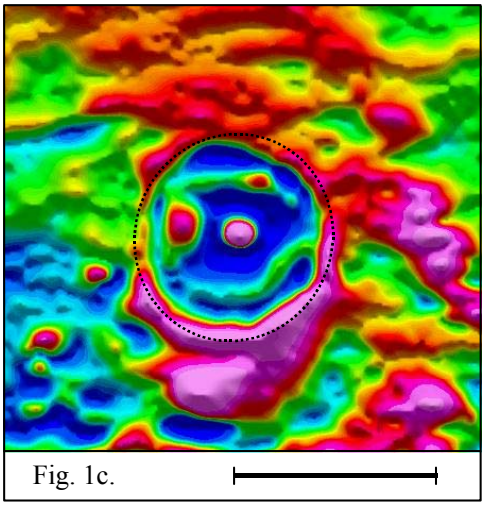

Figure 1: Images of residual magnetic data for (a) Yallalie (b) Foelsche and (c) Wolfe Creek. A dotted line shows the extent of each crater. The scale in the lower right of each figure represents 1 km.

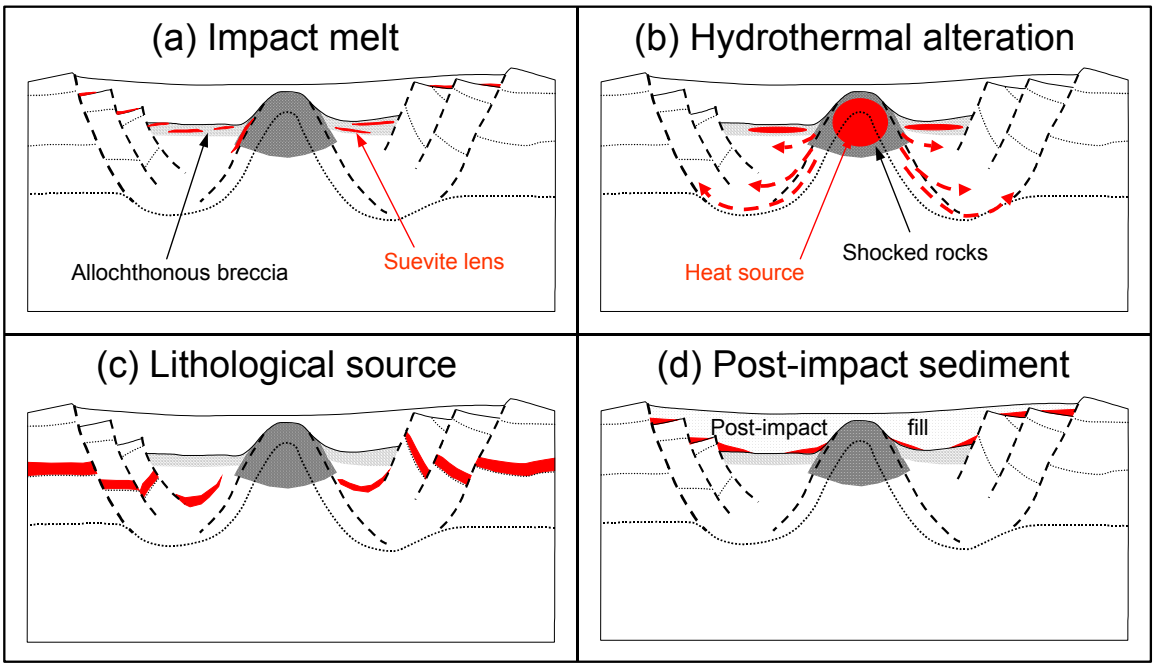

Figure 2: Methods of producing circular magnetic anomalies in impact structures.

SHOCK EFFECTS AT INCLINED MATERIAL INTERFACES — NUMERICAL SIMULATIONS. J.–M. Hertzsch, *Institut für Mineralogie, Museum für Naturkunde, Humboldt–Universität, Invalidenstraße 43, 10115 Berlin, Germany (h2808i3j@rz.hu-berlin.de).*

Introduction: A phenomenon in high velocity impacts which is still not completely understood is the occurrence of localised deformations, melt veins, melt dikes, and localised formation of high–pressure phases in impact crates, namely close to interfaces of different lithologies. Furthermore, the micromechanical properties of the materials and their effects on the propagation of shock waves determine the macromechanical behaviour of rocks subject to meteorite impacts. In order to study these phenomena, laboratory experiments [1] on samples composed of two different rocks and numerical simulations [2,3] of comparable situations have been carried out for a small number of configurations. Under the conditions present in the experiments and in the simulations, the materials do not melt by shock heating alone. However, considerable shear takes place at the interface of different materials and leads to additional temperature increase. In anticipation of planned further laboratory experiments, and in order to examine the effect of the angle between shock wave plane and interface between different materials, computer simulations of shock waves passing inclined material interfaces have been performed, and some results are presented here. Special attention is given to shock–induced temperature changes in the material.

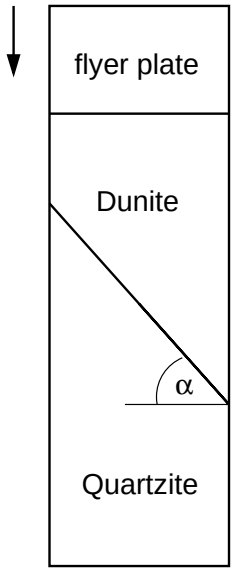

Figure 1: Probe geometry at impact.

Simulations: A two–dimensional Eulerian version of the hydrocode SALE [4] is used which has been enhanced to compute mixed cells containing two materials. Therefore the simulations were restricted to a system composed of dunite and quartzite. A 30 mm thick dunite flyer plate impacts a sample divided along an inclined interface into dunite and quartzite with a velocity of 2 km/s. The sample is 50 mm wide and 125 mm high. The geometry is shown in Fig. 1. The shock wave plane is initially parallel to the horizontal axis. The interface between the different materials cuts through the centre of the sample at varying angles α to the horizontal axis. Simulations have been conducted for $\tan\alpha \in \{0,\ 0.25,\ 0.5,\ 1,\ 1.5\}$. The resolution of the simulations is 200 cells in horizontal and 620 cells in vertical direction. Heat conduction has been neglected because of the short timescale of the shock passage. Because phase transitions may occur in the target [3], the equation of state must be able to describe such processes in a thermodynamically consistent way. Therefore, the ANEOS package [5] has been used to prepare tabulated equations of state which are used by the program. Figs. 2 and 3 show typical plots of plastic work and temperature in a vertical cross–section shortly after the shock has passed the centre of the sample for two selected values of $\tan\alpha$.

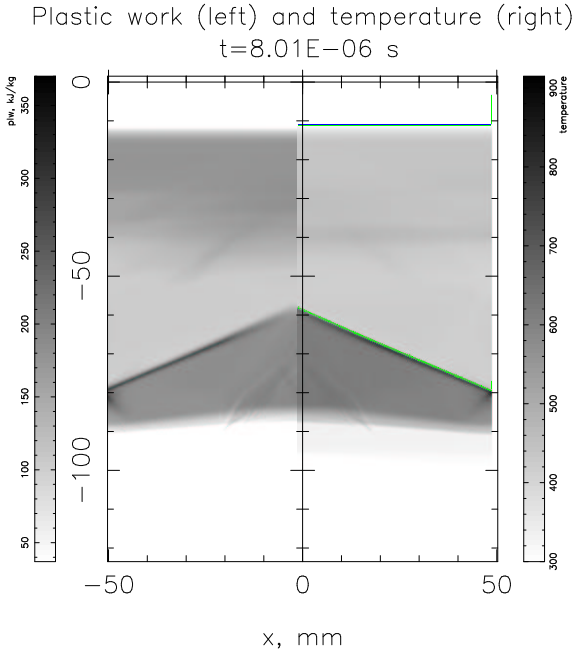

Figure 2: Plastic work and temperature 8 μs after impact for $\tan\alpha = 0.5$.

The present version of the code makes use of a very simple material model: The strength Y of the rock components is assumed to grow with pressure which is described in the Lundborg approximation [6]: $Y(p) = Y_0 + \frac{pk_p}{1+\frac{pk_p}{Y_m - Y_0}}$ where Y_m is a plastic shear strength limit at high pressure, and their shear strength is assumed to decrease to zero at melt temperature T_m [7]: $Y(p,T) = k_T Y(p,T_0)$ with a temperature coefficient $k_T = \tanh\left(\frac{E}{RT_M}\left(\frac{T_m}{T} - 1\right)\right)$. Thus, friction decreases

with rising temperature and reaches zero at melt temperature T_m. This results in a decrease of the heat production associated with shock compression and in a limited temperature rise. In consequence, the formation of melt zones by shock compression due to shear heating near the interface of two different materials can not be described properly, an additional mechanism of energy dissipation is needed to explain the experimentally [1] observed melting.

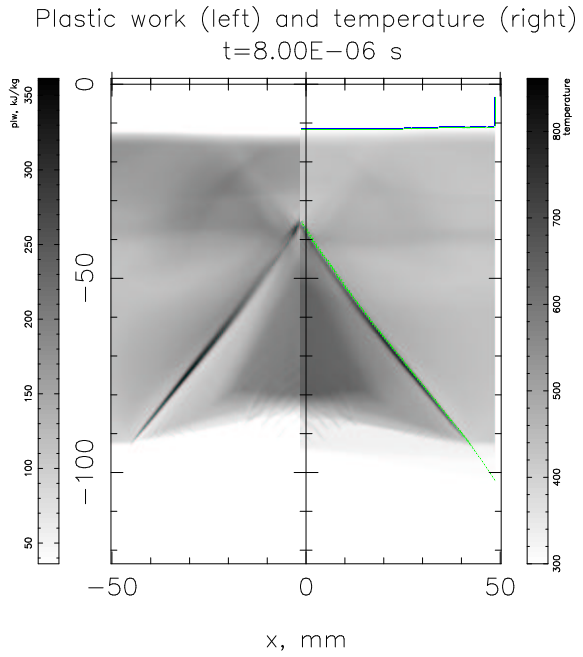

Figure 3: Plastic work and temperature 8 μs after impact for $\tan\alpha = 1.5$.

Results: Due to different propagation velocities in the materials concerned, the shock wave is refracted at their interface whose presence changes the direction of the shock propagation in the material below the boundary (see Figs. 2 and 3). In complex geometries, this can influence the degree of shock metamorphism at different places.

A concentration of plastic work and a considerable temperature rise above the average temperature in compressed quartzite is observed in an oblique zone in the neighbourhood of the material interface. It is observed that localised shear in particular at inclined boundaries between different materials results in a significant temperature rise and can make partial melting possible (depending on the parameters of the experiment). Pressure and temperature in the sample have been calculated. The maximum temperature at the interface has been extrapolated approximately from the simulation data and is shown in Fig. 4. It depends on the angle α between interface and shock front and appears to achieve its maximum for $\alpha = 45°$. This phenomenon should be studied in more detail.

Outlook: The effects of varying positions of material interfaces on the shock propagation and metamorphism in heterogeneous probes shall be studied experimentally and numerically in more detail. Future simulations must take into consideration effects of material strength and brittle fragmentation, and for a proper description of the melting process it is necessary to include the viscous behaviour of the material (in particular near the melting point) as a further source of energy dissipation. The temperature dependence of maximum shear stress, the kinetics of melt production and the viscous relaxation time of the material need also to be taken into consideration. Three–dimensional simulations are needed for a full description of the experiments where the samples have cylindrical shape because of manufacturing reasons.

References: [1] Kenkmann, T. et al. (2000), *Meteoritics & Planet.Sci. 35*, 1275–1290. [2] Heider, N. and Kenkmann, T. (2003), *Meteoritics & Planet.Sci.*, submitted. [3] Hertzsch, J.–M. et al. (2002), *Advances in Impact Studies, Lecture Notes in Geosciences*, submitted. [4] Amsden, A. A. et al. (1980), *Los Alamos Scientific Laboratory Report LA-8095.* [5] Thompson, S. L., Lauson, H. S. (1972), *Sandia National Laboratory Report SC-RR-71 0714.* [6] Lundborg, N. (1968), *Int. J. Rock Mech. and Mining Sci.* 5, 427–454. [7] Ohnaka, M. (1995), *Geophys. Res. Lett.* 22, 25–28.

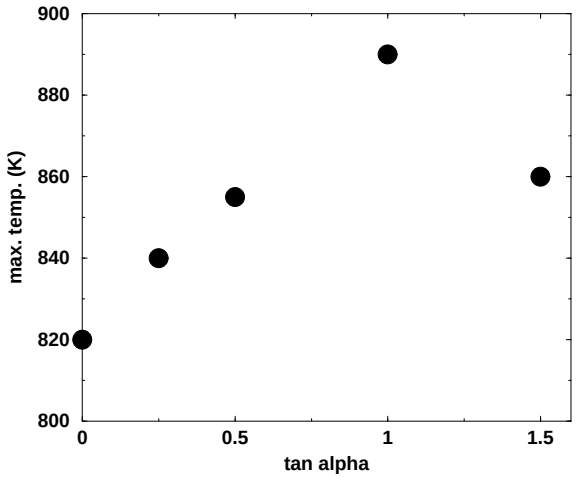

Figure 4: Approximate maximum temperature reached during passage of the shock front at the material interface over $\tan\alpha$. At $\alpha = 45°$, heating is strongest.

CHICXULUB CRATER STRUCTURE REVEALED BY THREE DIMENSIONAL GRAVITY FIELD MODELLING. A. R. Hildebrand[1] , J. D. Millar[1], M. Pilkington[2], D.C. Lawton[1] , [1]Department of Geology and Geophysics, University of Calgary, 2500 University Drive NW, Calgary, AB, Canada T2N 1N4 hildebra@geo.ucalgary.ca, millar@geo.ucalgary.ca, dclawton@geo.ucalgary.ca; [2]Geological Survey of Canada, 615 Booth Street, Ottawa, ON, Canada K1A 0E9 mpilking@nrcan.gc.ca.

Introduction: The structure of the Chicxulub crater has been actively investigated by potential field modeling, seismic reflection and refraction surveys, and drilling during the decade since its recognition as the crater responsible for mass extinction which terminated the Cretaceous Period. We have undertaken 3D modeling of the gravity field over the crater to refine our working structural model [e.g. 1, 2], and to compare our results with those of another 3D modeling effort [3]. The 3D gravity model also establishes an interesting target for scientific drilling.

3D Gravity Modelling: The 3D gravity modeling method employed is that of [4]. In this forward modeling procedure body geometry is specified using horizontally oriented polygons at arbitrary depths. The calculated field is integrated exactly in x and y, and then integrated across the third dimension, depth (z). The grid size was limited to 50 by 50 stations for computational practicality.

Gravity data: The gravity data compilation used (Figure 1) is based on land data collected five decades ago by Pemex (we have digitized unpublished Pemex maps filling in data gaps), results of an airbourne gravity survey conducted for Pemex which fills a data gap west of the crater, several recent land surveys (which have more than doubled available station coverage over the crater), and a shipbourne survey (which has filled in data gaps over the submarine portion of the crater). We have found that recently acquired density constraints have led to substantial revision of our initial 2D gravity models, but anticipate additional progress in improving the validity of gravity models with additional constraints. The Bouguer gravity anomaly expression of Chicxulub has a magnitude of up to ~30 mGals, but still suffers interference from regional anomalies unrelated to the crater; we have removed the regional anomalies guided in part by the regional crustal magnetic anomalies.

Model Results: The 3D modelling results (Figure 2) are particularly informative for the central structures of the crater. The central uplift (Figure 3) is revealed as a twin peaked structural high with vergence towards the southwest as previously indicated by 2D models [1] and consistent with seismic refraction results [5]. A "tongue" of the central uplift extends towards the northeast, in contrast to the steep gradients that bound it to the southwest. The width of the uplift at 4 km depth is ~45 km broadening to ~70 km at 9 km depth consistent with but slightly wider than previous 2D model results. The latter uplift diameter is comparable to that now exposed at Vredefort Dome suggesting that the latter structure is of comparable size to Chicxulub if its erosional level is ~10 km. The twin tops of the central uplift rise through the melt sheet to ~2 km depth for the density contrasts chosen. Choosing larger densities for the central uplift will allow for deeper tops to satisfy the central gravity high, but plausible limits still result in a relatively shallow depth for this feature, making it an achievable target for scientific drilling. This is in contrast to the results of [3] where a central uplift top of ~4 km was obtained; the difference seems to largely stem from the level of detail in the modeled data. More variability would be permitted in the model, but the independent constraint on the width of the central uplift from seismic refraction work [5, 6] removes greater widths as possibilities. The twin peaks of the central uplift have an axis of symmetry oriented SW-NE, indicative of the direction of a slightly oblique impact. The impact direction was towards the northeast based on the asymmetries preserved in various of Chicxulub's structural elements in addition to the vergence observed in the central uplift: compressional structures outside the crater rim, the rim uplift, compressional deformation preserved in the slumped blocks, morphology of the peak ring, off center position of the central uplift in the collapsed disruption cavity (CDC), elongated CDC, and initiation of slumping of Cretaceous stratigraphy off the Yucatan platform. This oblique impact is at a much steeper angle and at right angles to that proposed by [7].

The shape of the modelled central uplift is radically different from that advocated by [8] who proposed a cup shaped central uplift (concave top) with a top at ~3 km depth, but of similar width. That interpretation was apparently based on extrapolating discrete inferred high velocity anomalies in the area of the central uplift [9] into an annular ring. Possibly two of these velocity features result from detecting the twin tops of the central uplift, but if the other features are real it would require substantial departure from density–velocity relations in the rocks of the central uplift, and we doubt that the central uplift has an annular top.

The filling of the CDC, which is presumed to be largely melt, is revealed as a body slightly elongated in

a NE-SW sense (Figure 3) with a size only slightly smaller than previous 2D results. A depth for the melt sheet base of ~4 km is obtained consistent with the result of [4]. This depth is dependent upon the density contrast used (-0.15 g/cc) from values measured at the melt sheet top, however, and all the mass deficiency need not be melt. We note that seismic refraction detects a melt sheet contrast for only 1 km thickness [5]. The derived melt volume is 1.5 X 10^4 km^3, only slightly smaller than that of [4] and in good agreement with melt sheet volumes estimated by a variety of methods [10], although at the low end of the range of published estmates which go to 30X larger.

Acknowledgements: We are grateful to Petroleos Mexicanos, Instituto Mexicano del Petroleo, National Imaging and Mapping Agency, A. Camargo-Zanoguera, R.T. Buffler, and G. Kinsland for provision of gravity data, and to R. Cooper, J. Halpenny and other members of the gravity group of the Geodetic Survey of Canada, C. Ortiz-Aleman, R.E. Chavez, and J. Urrutia-Fucugauchi at UNAM, E. Graniel-Castro and A. Camara-Zi at UADY, and M. Connors at Athabasca University for data collection and survey support.

Figure 1: Gravity anomaly compilation over the Chicxulub crater; Bouguer gravity anomaly over land and free air anomaly offshore. Cool colours are lows, warm colours are highs; the coastline is indicated by a white line. White arrow indicates the direction of the non vertical motion of the impactor (from southwest to northeast).

Figure 2: Results of 3D model calculation with same colour convention.

Figure 3: Bounding surfaces of the modeled central uplift and melt sheet filling the CDC. Labelled contours indicate depth below surface.

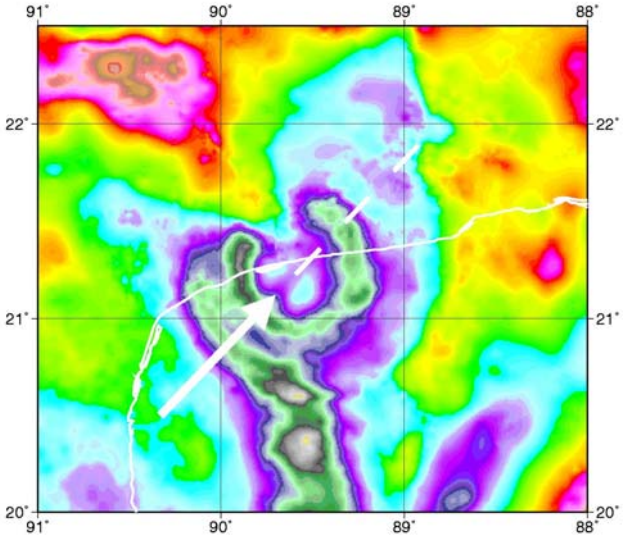

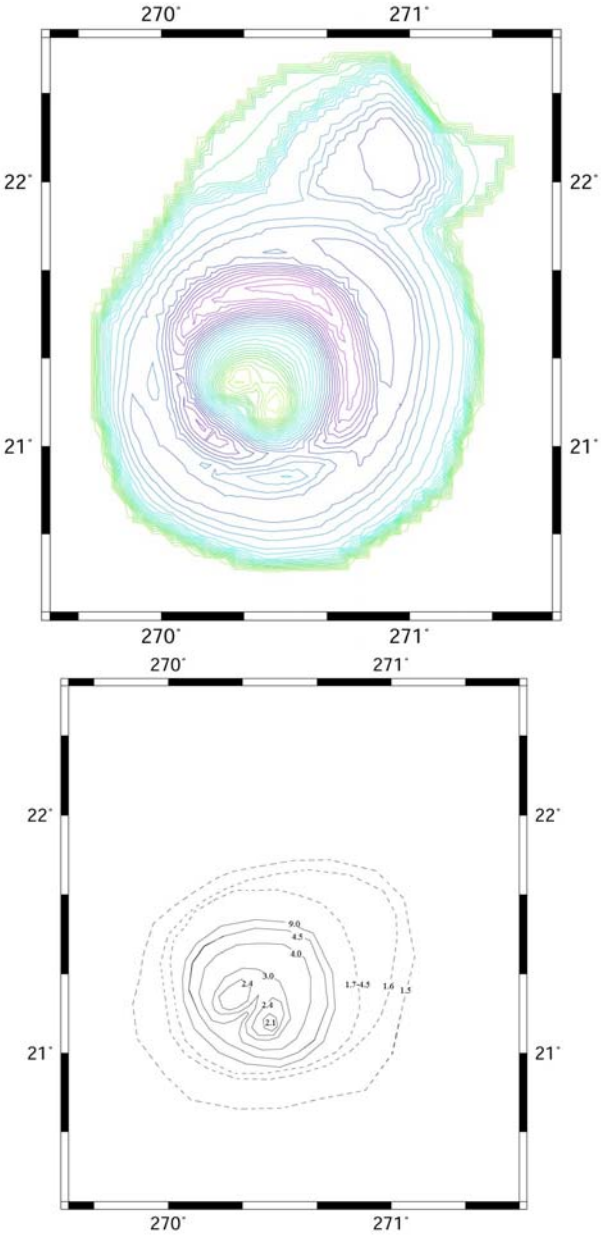

References: [1] Hildebrand, A.R. et al. (1998) in *Meteorites: Flux with Time and Impact Effects.* Pp. 153-173, Geol. Soc. Lond. Spec. Pub. 140. [2] Pilkington, M. and Hildebrand, A.R. (2000) *JGR 105,* 23,479–23,491. [3] Ebbing, J. et al. (2001) *Planet. & Space Sci. 49,* 599-609. [4] Talwani, M. and Ewing, E. (1960) *Geophysics, 25,* 203–225. [5] Christeson, G.L., 1999, *Geol. Soc. Am. Spec. Pap. 339*, 291-298. [6] Christeson, G.L et al. (2001), *JGR 106*, 21,751-21,769. [7] Schultz, P.H. and D'Hondt, S. (1996), *Geology, 24*, 963-967. [8] Morgan, J.V. et al., (2002), *Geol. Soc. Am. Spec. Pap. 356*, 39-46. [9] Morgan, J.V. et al., (2000), *LPI Contribution No. 1053*, 144-145. [10] Pilkington, M. et al. (1994) *JGR 99*, 13,147-13162.

RECENT RESEARCH IN THE CHESAPEAKE BAY IMPACT CRATER, USA—PART 2. REWORKED EJECTA AND IMPACT DEBRIS. J.W. Horton, Jr.[1], G.S. Gohn[1], L.E. Edwards[1], J.M. Self-Trail[1], D.S. Powars[1], M.J. Kunk[2], and G.A. Izett[3], [1]USGS, MS 926A, Reston, VA 20192, [2]USGS, MS 963, DFC, Denver, CO 80225, [3]Dept. of Geology, College of William and Mary and USGS Emeritus, 3012 East Whittaker Close, Williamsburg, VA 23285.

Introduction: The Chesapeake Bay impact structure on the Atlantic margin of Virginia, USA, is a late Eocene, 85-km-wide, complex crater formed in a continental-shelf environment. The "wet" target consisted of seawater (~300 m) underlain by lower Tertiary and Cretaceous unconsolidated sediments (400 to >750 m) and crystalline basement. A 38-km-wide, excavated inner crater is surrounded by a flat-floored annular trough, which has an outer rim of collapsed fault blocks. These features are surrounded by concentric faults and preserved beneath 150-400 m of post-impact sediments. In the annular trough, pre-impact Cretaceous sediments now constitute parautochthonous unit A that is block faulted, locally fluidized, and gradational upward into unit B that shows extensive fluidization, infiltration, and mixing. The disrupted pre-impact sediments were scoured and covered by seawater resurge deposits of the Exmore diamicton. The Exmore consists of mixed Lower Cretaceous to upper Eocene sediment clasts (up to boulder size) and minor crystalline-rock clasts in a matrix of glauconitic, quartz-rich, muddy sand that contains Cretaceous, Paleocene, and Eocene fossils [1,2]. Recent drill cores from the western annular trough at Bayside (728.5 m deep), the NASA Langley Research Center (635.1 m deep), and North (435.1 m deep), and a core from the outer rim at Watkins School in Newport News (300.3 m deep), are 8, 19, 24, and 27 km, respectively, outside the inner crater. All four cores penetrated the Exmore diamicton, and cores from Bayside and Langley sampled complete post-impact and crater sections down to Neoproterozoic granites of a peri-Gondwana basement terrane [1].

Reworked Ejecta and Debris: Planar deformation features (up to 5 intersecting sets) characteristic of shock metamorphism in quartz occur in rare grains or rock fragments from the Exmore of all four cores, confirming earlier evidence of the Exmore's hybrid impact origin. The proportion of shocked to unshocked quartz grains in the Exmore matrix is very low, indicating that the shocked grains are diluted by an enormous volume of other sediment. This proportion is consistent with the character of the Exmore as a mixed sedimentary deposit that contains ejecta, although a simple ejecta blanket is not intact in the cores. Most crystalline clasts in the Exmore diamicton and underlying sediments are rounded, detrital, and essentially undeformed, but a few have angular shapes and cataclastic fabrics. Shocked quartz is an integral part of the cataclastic fabric in some clasts, indicating that this fabric was produced by the same impact event. Fractured calcareous nannofossils and fused, bubbled, and curled dinoflagellate cysts occur in the Exmore matrix, where coexistence of these highly unusual, degraded microfossils and shocked quartz particles indicates an impact origin [3,4]. The unusual damage preserved in these marine microfossils may record conditions of heat, pressure, or abrasion during the oceanic impact.

Sampling Tool: The impact event provided a remarkable sampling tool by excavating an enormous volume of target rock, including little known basement terrane(s), and scattering fragments where they can be retrieved at shallower levels. Crystalline rock fragments interpreted to be ejecta include a variety of felsic to mafic plutonic rocks and felsite. In the Langley core, these fragments consist of a single rock type (felsite) in contrast to more diverse assemblages in other cores, indicating that ejecta were distributed unevenly, perhaps in rays. Microspherulitic matrix in some felsite clasts is evidence of the devitrification of either impact melt or older volcanic rock. The largest impact-derived rock fragments are in the lower part of the Exmore diamicton, suggesting that, in some areas, the Exmore is a single, crudely graded deposit. Shocked quartz in a felsite clast several meters below the Exmore supports other evidence for infiltration of sediment from the diamicton into the underlying unit B. The Ar-Ar age spectrum of white mica from a cataclastic leucogranite clast in the Exmore diamicton is consistent with Neoproterozoic U-Pb ages of cored basement granites, and an Ar-Ar age spectrum for K-feldspar indicates final cooling through ca. 150°C closure at about 255 Ma [1] without discernible impact heating. Deep coreholes in the central part of the crater are needed to study impact products and processes not documented in previous coreholes.

References: [1] Horton J. W. Jr. et al. (2002) *GSA Absts. with Progs.*, 34, 466. [2] Edwards L. E. et al. (2002) *GSA Absts. with Progs.,* 43, 465-466. [3] Self-Trail J. M. (in press) *Geology*. [4] Edwards L. E. and Powars D. S. (2003) *Palaios*, 49, 275-285.

DISTRIBUTION AND ABUNDANCE OF DARWIN IMPACT GLASS. K.T. Howard[1] and P.W. Haines[1]
School of Earth Sciences, University of Tasmania, Box 252-79, Hobart, Tasmania, 7001, Australia. kthoward@utas.edu.au

Introduction: Since its first discovery in 'soils' near Mt Darwin, western Tasmania, Australia, impact glass has been reported across an area of about 400 km^2 [1,2]. Across much of this area Darwin glass appears to be patchily distributed and its distribution is poorly defined. We have improved the constraints on the dimensions of the strewn field and estimated the abundance of glass.

Stratigraphic setting of Darwin glass: Across the strewn field the glass is intimately associated with quartzite gravels. The gravels are residual deposits formed largely from the *in situ* weathering of quartz veins in country rocks. Transport of the quartz fragments, especially in flat areas has largely been vertical. Glasses recovered from these gravels show fine surface sculpting and delicate primary morphologies that further suggest both the glass and therefore the gravels have not undergone significant lateral movement or spent time entrained in fluvial transport. As residual deposits the nature of the glass bearing gravel horizons is strongly influenced by elevation and topography.

Slopes and flat ground between ~230–500 m: On steep and gentle slopes and flat lying ground between approximately 230 and 500 m elevation the glass bearing quartz gravel lies beneath a layer of soil and peat. Immediately below the peat are the largest quartz fragments and glass in a matrix of fine quartz sand that extends to the contact of the highly weathered bedrock. Glass is rare in the fine sand below the larger quartz fragments. The peat layer varies in thickness but is typically around 20 cm thick and free of glass fragments. Below the peat the thickness of the glass bearing gravel horizon ranges from a few centimetres to several metres. On low and mid slopes the gravel horizon is consistently around 30 cm thick. The thickest gravel horizons tend to be on gentle and flat lying ground at lower altitudes.

Peaks >500 m: Peat is absent on hills and on mountain summits in the strewn field and the gravel horizon is also either absent or confined to isolated free quartz fragments and rare Darwin glass sitting directly on weathered bedrock. Previous workers assumed that early Holocene ice accumulation and transport had removed Darwin glass from slopes above 500 m.

Valley floors < 220 m: On valley floors in the strewn field the gravel horizon and Darwin glass are not exposed - buried under peat and valley filling sediments - or have been incorporated in extensive deposits of re-worked glacial moraine. Rare fragments of glass have been found sitting atop of valley fill sediments on the crater floor and these have been moved down slope.

Dimensions of the strewn field: Figure 1 shows all sites where *in situ* Darwin glass has been found (solid circles). The map is a composite of sites discovered and or studied in detail here and those reported in previous works. Verified anecdotal reports of glass finds are also included. Attention was focused on delineating the outer limits of glass occurrences in all directions. Sites where residual gravels were searched and found to be glass free are indicated (Fig. 1, x's) and these are sites that are interpreted to define the approximate limits of the strewn field (Fig 1, solid line). The southern and eastern limits of the field are least well defined and further access in these directions is difficult. Glass is likely to be found further south but to the east residual deposits are very rare and no glass is found. The suspected source crater sits at the apparent eastern limit of the field. This asymmetry in the distribution of glass noted by [2] is interpreted to reflect the preservation of glass only and not its primary post impact distribution. The asymmetry is derived from the presence of Engineer Range. These mountains (Fig. 1, triangles) are drained on either side by major rivers that have transported away glass eroded from the slopes. The glass distribution relative to the suspected crater is more equal in the remaining directions and covers and area of over 410 km^2.

The abundance of Darwin glass: At 8 sites surrounding the suspected crater and defining an area of 10 x 5 km controlled excavations have been conducted in order to estimate the abundance of glass present. A controlled excavation refers to an archaeological style dig where a known volume of material is sieved and searched for recovered glass. At each site 0.03 m^3 (10 standard prospectors' pans) of glass bearing gravel was sieved through 1 and 0.5 cm mesh sieves. Where possible the material was excavated from a standard sized area usually around 1 m^2 however, dense vegetation with complex root systems and steep rugged terrain often prevents this control. All visible glass was recovered from the sieves and a ground sheet placed below sieving operations searched for fine glass fragments. Recovered glass fragments were weighed and results normalised to kg/m^3. The determined glass abundance ranges from 47 to 0.3 kg/m^3 across the study area. The maximum value is reached in a thick residual gravel deposit some 2 km from the suspected crater. At the remaining sites measured abundances are more consistent and there is a general trend of decreasing glass abundance away from the crater. Outside of this 50 km^2 study area the abundance of glass in grav-

els is too low, or distribution too patchy, or access too poor for glass to be recovered in controlled conditions. Here glass is only recovered by fossicking without consideration of the volume of material or area searched and the abundance of glass is difficult to quantify.

Melt Volume: By estimating the average thickness of the gravel deposits across the 50 km^2 study area the volume of ejected melt can be approximated. Most of the survey area is covered with peat above the glass bearing gravel horizon that is consistently around 30 cm thick. In contrast at other locations several metres of glass bearing gravel exists and on peaks the horizon is typically less than 1 cm thick. After accounting for thin gravel cover on peaks, a conservative estimate of the average thickness of the glass bearing gravel horizon in the study area is taken to be 15 cm. Excluding the most abundant site (47 kg/m^3) the average abundance of glass in the gravel deposits across the survey region is 3.4 kg/m^3. Therefore, in this 50 km^2 area it can be estimated that there is approximately 25 500 tonnes of glass. Assuming a SG of 2 this represents a melt volume of 11100 m^3 or 0.00001 km^3. Errors in estimating the average thickness of the gravel horizon strongly influence melt volume determinations but these estimates of the gravel horizon thickness and the abundance of glass in the horizon are both conservative. As the survey area represents only $1/8^{th}$ of the strewn field the estimated melt volume herein is considered to be very much a minimum estimate.

Discussion: at 1.2 km in diameter Darwin Crater is at the lower limit of scaling equations that model melt production. Based on the equation of [3] approximately 0.0012 km^3 of melt can be expected to be produced during excavation of a 1.2 km diameter crater. Of this around 1% - 3% of fully melted material (0.00001 km^3 or 12000 m^3) is expected to be ejected further than a few crater radii [3,4,5]. This agrees well with the measured minimum estimate of the volume of glass in the study area (0.00001 km^3). If the remaining >350 km^2 of the strewn field is considered modelled estimates of ejected melt volume are significantly too small. For other studied craters and especially those in sedimentary rocks modelled melt volumes generally far exceed measured volumes [3,6]. This indicates that relative to the size of the suspected source crater this is the most abundant ejected impact glass on Earth! In fact the volume of ejected melt at Darwin Crater is more abundant than is observed at much larger complex craters. Zamanshin Crater (13 km diameter) is more than 10 times larger than Darwin but here it is estimated by [7,8] that there is less than 100 tonnes of ejected glass – orders of magnitude less than is observed in the Darwin glass strewn field and importantly both glasses are of almost the same age. At similar sized simple craters such as Meteor or in small crater fields like Henbury far less glass has been found and all of this has come from closer to the crater than at Darwin [6,9]. This is despite these craters being on easily searched, flat desert planes in contrast to the mountainous rainforest of the Darwin glass strewn field. Acid groundwater ideal for the preservation of glass exists across the study area. However, this high abundance of Darwin glass seems unlikely to relate to preservation only and rather is interpreted to reflect more efficient than expected production of ejected melt during the impact event. The distribution of the glass that extends over a distance of more than 20 crater radii also exceeds modelled expectations and field observations of impact glass distribution [4,9]. This range is typical of the distribution of tektites from large impact events but the bulk of Darwin glass has a morphological and chemical character more commonly associated with *proximal* impact glasses.

Implications: My observations indicate that the crater structure is almost completely lacking in glass and this would support the findings of [3,5] that in smaller impacts a lesser volume of melt is produced but a greater proportion (all?) of this melt is ejected. The crater is in metasedimentary rocks and as such these data also appear to support the notion that the high volatile content of sedimentary rocks results in the unusually wide dispersion of melt [6]. This is contrary to recent observations at large craters in sedimentary rocks by [9] and may reflect differences in the cratering mechanics between small simple and larger complex craters. Alternatively there may be a larger undiscovered source and observed trends in the variation in glass are coincidental only - current work is aimed at determining the structur ıd its relationship to Darwin glass.

Fig. 1.

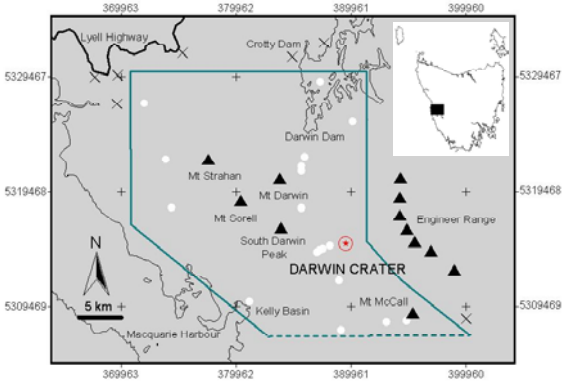

References: [1] Ford, R.J. (1972) *EPSL*, 16, 228-230.[2] Fudali R.F. & Ford, R.J. (1979) *Meteoritics*, 14, 283–296.[3] Grieve, R.A.F. & Cintala, M.J. (1992) *Meteoritics*, 27, 526-538.[4] French B.M (1988) *LPI Contribution No. 954*.[5] Orphal, D.L. et al. (1980) *LPS XI*, 833-5.[6] Kieffer, S.W. & Simonds, C.H. (1980) *Rev. Geophys. Space Phys*, 18, 143-181. [7] Florensky, P.V. (1976), *LPI Contribution No.259*, 33-35. [8] Masaitis,V.L. (1984) *LPS XV,* 515-516 [9] Osinski, G.R. et.al (2003*) ICBG Abstract # 8009.*

LARGE IMPACT CRATER MODELING: CHICXULUB. B. A. Ivanov, Institute for Dynamics of Geospheres, Russian Academy of Science, Leninsky Prospect, 38-1, Moscow, 119334, Russia (baivanov@online.ru, ivanov@lpl.arizona.edu).

Introduction: Every crater on Earth has its own specific. To model observed geological structure and geophysical anomalies one should tune a lot of model parameters without any guarantee the model in use is adequate to describe all involved natural processes. To start the process of modeling we need to make the first step using the "standard" model based on first principles and laboratory data. The answer may be not very spectacular. However, only after the "standard" modeling we can realize what else should be added for better understanding of what we see in the field. We present results of a "standard" numerical modeling for Chicxulub.

Numerical Model: The solver for differential equation of motion of a continuos media used is the heavily modified SALE code, primarily designed for modeling of fluid motion [1]. The deviator stress description (necessary to model elastic-plastic behavior and brittle failure of rocks) has been added by Melosh [2]. In addition the possibility to use tabulated equation of state and two materials(and vacuum) treatment in the Eulerian mode has been added. The latter additions yet to be presented in details (see first results [3,4]). The Eulerian multimaterial version of SALE is named SALEB.

SALEB can treat simultaneously 2 materials and vacuum. In respect to the Chicxulub modeling it is not enough as the simplest modeling should include atmosphere, 2 kinds of sediments, crust and mantle. To study general scenario of a crater formation one can use 2-layer target: sediments+crystalline basement or crust-mantle target. Here we present the modeling of a crust+mantle target. The sedimentary layer is described with a crust mechanical parameters. However the displacement of the would be sedimentary layer is presented with so called tracer particles which allow to trace displacement of selected zones (for example, layers) in a target.

Tabulated equations of state (EOS) are computed separately with the ANEOS Fortran code [5] with input parameters from [6] for granite and dunite, simulated crust and mantle.

Strength properties of granite and dunite are corresponds to published triaxial tests of specimens to present shear failure and post-failure dry friction in rocks. Thermal softening model [8] is used to represent gradual decrease of strength and friction as temperature approach the melting point.

The collapse of large impact crater assume an additional (to the thermal softening) temporary friction reduction in fragmented rocks around a growing impact crater. The acoustic fluidization (AF) model [9] is used in a "block oscillation" flavor [10, 11] The primary choice of AF model parameters is done with a linear scaling model [12].

Crater Size: It is not an easy problem. Chicxulub looks like a rim-less crater in contrast, for example, to Venusian craters of a similar size. A similar craters on Venus has a depth of 1 km [13]. Chicxulub measured with a Cretaceous surface (CS) is of 700 m maximum from 3D geophysical model [14]. Additional constraints for the modeling are deduced from the interpretation of a seismic survey [15]: assumed CS is traced as close as 40 km to the center in the form of slumped megablocks. The summary of drilling in Chicxulub [16] is in a good agreement with [14, 15]. For these reasons we made a parametric analysis of the projectile diameter, D_{pr}, shape and impact velocities, v, in the range of 12 to 25 kms^{-1} (totally 15 model runs). Selected results are presented in Fig, 1 and Table 1.

The "impact parameter" $L = D_{pr}\, v^{0.58}$ [17] is used to compare different impact velocities.

Modeling results: Results shown in Fig. 1 and Table 1 in general show a deviation from the widely accepted scaling law for the transient cavity [18] and Croft's phenomenology collapse rule [19]. Partially it results from the presence of a more competent mantle 33 km below the surface.

The best to date fit to geologic and geophysical data is obtained for a model run where the projectile 14 km in diameter (granite EOS) strikes the surface at 12 km s^{-1} . Similar results may be produced with a smaller projectile at higher impact velocity. The modeled crater (as in all other runs) has an elevated rim ~800 m above the pre-impact surface. The rim crest diameter is about 172 km with an apparent diameter (at the level of the pre-impact surface) of 144 km. In respect to this model crater the Yax-1 site is close to the inner crater slope. The crater depth is around 1 km: larger than Chicxulub CS depth according to [14]. The maximum transient cavity depth is about 29 km, and the maximum transient cavity volume is of 48,000 km^3. The final crater volume is 3 to 4 times smaller.

The transient cavity collapse results in the central uplift dynamic "overshoot" as high as ~20 km above the surface. During the central uplift collapse high temperature and melted material creates an intensive

outward motion - this motion definitely create the flow structures at the final crater floor. The volume of impact melt is of the order of 6,000 to 10,000 km^3 - in an approximate concord with estimates in [14]. Most of basement melt is trapped inside the crater cavity.

The pre-impact (CS) is subsided to a depth of 5 km, having a hinge at the distance of 45 km from the center. The circular trough above the CS is filled with overturned sediments and the material of the collapsed central uplift. All these details are in an approximate agreement with available observations.

Larger impacts produce more impact melt (10,000 to 12,000 km^3), however the ejecta layer is much more thick (last row in Table 1) in a visible discordance with drilling data. Smaller impacts produce too small amount of the impact basement melt (~3,300 km^3 for the crater with a rim diameter of 156 km) what is close to observed 2,000 km^3 in the Popigay crater (D~100 km).

In addition to morphologic features and melt production many other model results may be discussed in parallel with observation data.

Conclusion: With available numerical models it is possible to simulate a crater similar to Chicxulub in many details (Fig. 3). 2D simulations presented here create a solid basis for much more time consuming 3D simulations. Future study should be targeted to explain the visible absence of an elevated crater rim in Chicxulub (erosion vs specific crater formation in a shallow see). Also a lot of model parameters may be tuned by comparison with observations.

Acknowledgements: The author is supported with the RFBR project # 01-05-64564-à.

References:

[1] Amsden, A. et al.. (1980). *Los Alamos National Laboratory Report LA-8095*, Los Alamos, NM, 101pp. [2] Melosh et al. (1992) *JGR* 97: 14,735-14,759. [3] Ivanov B. A. et al. (1997) *Intl. J. of Impact Eng.* 20: 411-430. [4] Ivanov B. A. et al.(2002) Geol. Soc. Amer. Spec. Paper 356: 587–594. [5] Thompson, S. L., Lauson, H. S. (1972) Sandia National Laboratory Report SC-RR-71 0714. [6] Pierazzo E. *et al*. (1997) *Icarus* 127, 408-422. [8] Ohnaka, M. (1995) *GRL* 22: 25-28. [9] Melosh H.J. (1989) *Impact cratering: A geologic process*. Oxford University Press, 245 pp. [10] Ivanov B. A. and Kostuchenko V. N. (1998) *LPSC* 29th, #1654. [11] Melosh H. J., Ivanov B. A. (1999), *Annu. Rev. Earth Plant. Sci.*, 27, 385-415. [12] Ivanov B. A. and Artemieva N. A. (2002) *Geol. Soc. Amer. Spec. Paper* 356: 619–630. [13] Ivanov B. A. and P. G. Ford (1993) *LPSC XXIV*: 689-690. [14] Ebbing J. et al. (2001) *PSS* 49: 599–609. [15] Morgan J. V. et al. (2000) *EPSL* 183: 347–354. [16] Stöffler D. et al (2003) *LPSC* #1553. [17] Dienes J. K. and J. M. Walsh (1970) In *High Velocity Impact Phenomena* (R. Kinslow Ed.) Academic Press, NY, pp. 45-104. [18] Schmidt R. M. and K. R. Housen. (1987) *Int. J. Impact. Eng*. 5: 543-560. [19] Croft, S. K. (1985) Proc. 15th LPSC, JGR 90: C828-C842.

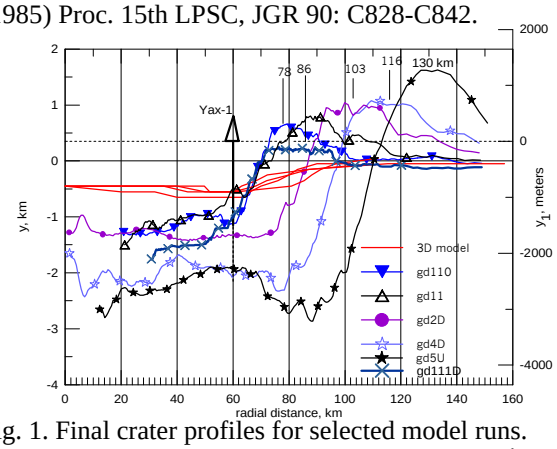

Fig. 1. Final crater profiles for selected model runs.

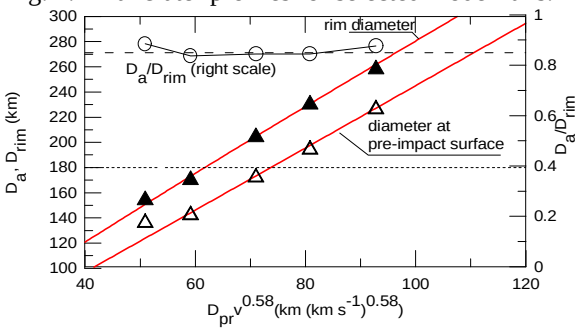

Fig. 2. Rim diameter and apparent diameter of the modeled crater vs dimensional "impact parameter".

Table 1. Crater diameters and ejecta characteristics at the distance of 60 km from the crater center.

Model run	Rim crest diameter, km	Apparent diameter, km	Effective ejecta thickness, m	Basement clasts fraction
gd111D	156	138	220	0.22
gd11	172	144	400	0.54
gd22D	206	174	2400	0.56

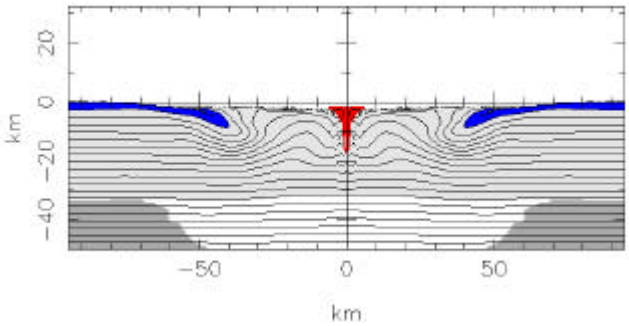

Fig. 3 The "best" modeled Chicxulub (600 seconds).Colors (top to bottom) are for sedimants, crust and mantle. Red is for the impact melt pool

LARGE SCALE IMPACTS AND TRIGGERED VOLCANISM. B. A. Ivanov[1,2] and H. J. Melosh[2], [1]Institute for Dynamics of Geospheres, Russian Academy of Science, Leninsky Prospect, 38-1, Moscow, 119334, Russia (baivanov@online.ru, ivanov@lpl.arizona.edu), [2]Lunar and Planetary Laboratory, University of Arizona, Tucson AZ 85721 (jmelosh@lpl.arizona.edu).

Introduction: The idea of impact induced volcanism continues to blossom ([1-3] and other references). However, this appealing idea is seldom supported with an appropriate physical mechanism. The aim of this publication is to critically examine some frequently cited mechanisms of impact energy transformation into a trigger for terrestrial volcanism and magmatism.

Close and Remote Action: In general, we can distinguish two groups of ideas about how volcanism might be provoked by impacts. The first one assumes that the uplift of geotherms accompanying the collapse of a giant impact crater leads to pressure release melting of deep mantle/asthenosphere layers. The second group includes volcanism triggered by seismic waves focused on the antipodal point of Earth.

We have recently reviewed the first ("close") group of "impact trigger volcanism" ideas [4, 5] and found that impacts small enough to be sufficiently frequent (final crater diameter of 250 km) do not uplift rocks from great enough depths to create melt by pressure release melting. Although larger impacts really can do the job, the number of possible impacts creating craters 300 km in diameter and larger is too small to be a common cause of most of the Earth's young hot spots.

Antipodal Seismic Shaking: The remote action of giant impacts is most frequently discussed in terms of seismic wave focusing near the antipodal (to the impact site) point of the Earth. A full analysis is not easy because it requires lengthy computations of the initial phase of impact, shock wave transformation into seismic waves, and the complex pattern of seismic wave propagation through Earth's inhomogeneous mantle and core. In addition, the mechanism(s) by which seismic shaking is converted into magmatic activity through partial melting in the asthenosphere must be treated. Here we present a simple estimate of the maximum ("optimistic") value of seismic energy dissipation in a viscous asthenosphere.

The approximate treatment of the impact energy-shock wave-seismic wave transformation was performed by Boslough et al. (1996). The results are very instructive: a Chicxulub scale impact (10 km diameter asteroid at an impact velocity of 20 km/s) is modeled with a hydrocode until the stress wave amplitude drops below the elastic limit. The elastic waveforms are used to construct the elastic solution, giving synthetic seismograms for the whole Earth, based on a layered 1D PREM model.

The main result is an estimate of the seismic wave amplitudes focused at the antipodal point (at an angular distance of 180 degrees). We use these results to estimate the energy dissipation in the asthenosphere.

We begin with a first-order approximate estimate. Despite relatively large displacements (± 10 m) strains in the antipodal point are small (~50 μstrain).

The maximum stress oscillation, of order 10 MPa (100 bar), is very small in comparison with the crust/mantle strength at a depth of 10 km and deeper. Consequently, an exact elastic solution gives no energy dissipation at all: elastic strains, by definition, are completely reversible.

We use the waveforms published by Boslough et al (their Fig. 3) in a model that estimates the largest possible heating effect. The largest amplitudes (~10 m amplitude at the surface) are concentrated in ~10 oscillations that last ~1000 second. The approximate period of oscillation T is ~100 second, corresponding to a wavelength of 700 km .

For such a long wave we can assume similar parameters in the asthenosphere (~200 km deep). With an average amplitude A of 10 m such oscillations have a typical (average) velocity <v> of material displacement of the order of

$$A/T=<v>= 0.1 \text{ m s}^{-1}$$

Strain rate may be estimated as

$$e' \sim du/dx = <v>/(c_L \times T) = 1.4\ 10^{-7}$$

where c_L is the longitudinal seismic wave velocity. The maximum strain during one period is

$$e' \times T = 1.4\ 10^{-5} = 14.3 \text{ μstrain}$$

close to the 50 μstrain estimated by Boslough et al.

For simplicity, we assume that this strain rate operates throughout all 1000 seconds of oscillations.

The widely cited estimate of mantle viscosity of 10^{20} Pa s is valid for slow deformation. The Maxwell time to use this viscosity is

$$\mu/G = 10^{20}/50\ 10^{9}=2\ 10^{9} \text{ seconds} = 63.5 \text{ years}$$

Assume that the upper asthenosphere is partially molten and therefore has a much smaller viscosity (and the same shear modulus). The maximum heating occurs when the Maxwell time is equal to the oscillation period of 100 seconds;

$$\mu = 5\ 10^{13} \text{ Pa sec}$$

The dissipative rate is $\mu \times e' \times e'=1.0$ W/m^3. Acting for 1000 seconds this gives an energy dissipation of 1000 J/m^3, corresponding to a heating of about 1 K in rock. However, in a partially melted material this

heating is manifested as increased melting, not only higher temperature. Using a melt entropy of 330 J/kg-K, the methods and thermodynamic data of Jull and McKenzie[13] predict a temperature increase of 0.4 K and a partial melt fraction increase of 0.1% for peridotite at 8 GPa (250 km depth) in response to this "optimistic case" heating.

Less "optimistic" estimates use the "quality factor", Q, of the Earth's (e.g. [7]). The value of Q^{-1} measures the amount of strain energy dissipated due to anelasticity per cycle of oscillations. For the PREM model the lowest Q value of 80 is listed for depths of 80 to 220 km. Thus, we can say that during 80 cycles the strain wave energy decreases e (= 2.71828) times. Ten main oscillations in the Boslough et al. model dissipate approximately $1 - e^{-10/80} \sim 13$ % of the energy. Taking wave specific energy as $\sigma \times e \times \rho^{-1}$ (stress×strain/density) one gets $1.5\ 10^{-1}$ J/kg for $\sigma \sim 10$ MPa and $e \sim 50\ 10^{-6}$. For a heat capacity of 1 kJ kg^{-1} this gives only ~0.15 mK assuming that all the wave energy is dissipated as heat (in partially melting rock the temperature and melt fraction are computed by scaling the result cited above to the lower energy input). More exact estimates should take into account that the asthenosphere thickness is less than the characteristic wavelength.

We conclude that the direct thermal action of a Chicxulub scale impact at the antipodal point is negligible. More elaborate mechanisms such as gas bubble growth, triggering of local earthquakes, etc. might be invoked as volcanic "triggers". However, the possible presence of "natural amplifiers" poses a problem for the "triggered volcanism" idea: Much more frequent natural earthquakes (perhaps occurring only close to the "pregnant" hot spot) may forestall the seismic action of rare giant impacts. Several triggering events due to remote earthquake have been analyzed recently [8, 9].

Cratering Rate on Earth: The above concerns with the strength of the thermal triggering effect for Chicxulub size impacts may be countered with the possibility that larger impacts would cause stronger shacking. In response we want to again emphasize just how rare giant impacts are.

Comparative studies of the impact crater records of terrestrial planetary bodies resulted in a more or less reliable understanding of the cratering rate from asteroids of a given diameter (see the recent review [10] and reference list therein). The lunar cratering curve, recalculated to Earth, gives a good estimate of how often large craters form (Fig. 1). The totally independent estimates [11] of the terrestrial crater size frequency distribution made with a "nearest neighbor" technique are in good agreement with the lunar-based model. Fig.1, constructed for the whole Earth's surface, shows the statistically largest crater for a given time period.

Large surface magmatic events occur, on average, every 20 Myr [12]. Hence, even if each (!) D~100 km impact crater provoked an antipodal magmatic event, large scale impacts are not frequent enough to be suspected in volcano ignition.

Acknowledgements: The work is supported by NASA grant NAG5-11493 and the Russian Foundation for Basic Science (project # 01-05-64564-à).

References: [1] Rampino, M. R. (1987) *Nature* 327: 468. [2] Jones A. P. et al. (2002) *EPSL* 202:. 551-561 [3] Abbott D. H. and A. E. Isley (2002) *EPSL 205: 53-62*. [4] Ivanov B. A. and H. J. Melosh (2003) *LPSC XXXIV*, #1338. [5] Ivanov B. A. and H. J. Melosh (2003) Impacts do not initiate volcanic eruptions I: Eruptions close to the crater. Submitted to *Geology*. [6] Boslough et al. (1996) *Geol. Soc. Am. Spec. Publ.* 307: 541. [7] Masters T. G: and P. M. Shearer (1995) In *Global Earth Physics. A Handbook of Physical Constants* (T.J. Ahrens Eds.), Washington, D.C., AGU, pp. 88-103. [8] Gomberg J. and S. Davis (1996) *JGR* 101: 733-749. [9] Gomberg J. et al. (2000) *Nature* 411: 462-466. [10] Ivanov B. A. et al. (2003) In: *Asteroids III* (B. Bottke, A. Cellino, P. Paolicchi, and R. Binzel Eds), Chapter #3025. [11] Hughes D. W. (2000) Mon. Not. Roy. Astron. Soc., 317, 429-437. [12] Ernst R. E. and K. L. Buchan (2003) *Annu. Rev. Earth Planet. Sci.* 31: 469–523 [13] Jull, M. and McKenzie, D. (1996), *J. Geophys. Res*. 101, 21,815-21,828.

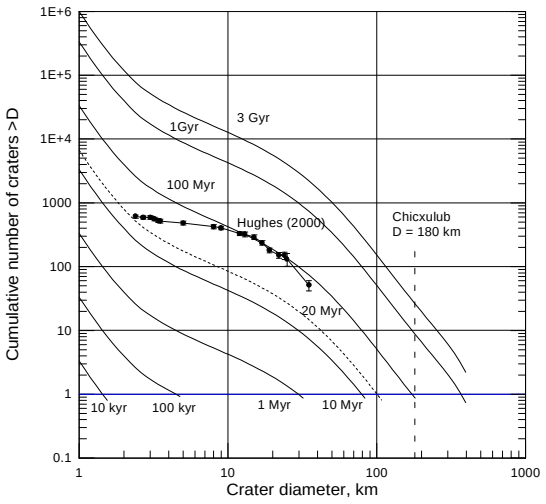

Fig. 1. The cumulative number of impact craters for the whole Earth for a given time period. A Chicxulub scale impact repeats on average every 100 Myr. During 20 Myr (the average time between LIP formation [12]) one 100-km crater, on average, is formed (dashed curve for 20 Myr). Data from [11] are shown for comparison.

THE LOCKNE CRATER: SHOCK COMPRESSION OF BASEMENT ROCKS AND EJECTED MATERIAL. B. A. Ivanov[1] , V. V. Shuvalov[1], and Maurits Lindström[2], [2]Institute for Dynamics of Geospheres, Russian Academy of Science, Leninsky Prospect, 38-1, Moscow, 119334, Russia (baivanov@online.ru, ivanov@lpl.arizona.edu, shuvalov@idg.chph.ras.ru), [2]Department of Geology and Geochemistry, Stockholm University, 106 91 Stockholm, Sweden (maurits.lindstrom@geo.su.se).

Introduction: The Lockne crater (D~7km) has been formed under 500 to 700 m of sea water. The previous field investigations and numerical modeling (see latest publications [1,2]) have revealed and explained several specific phenomena typical for the submarine impact cratering. Here we present some additional results of the numerical modeling targeted to expand the database for the comparison with geologic facts, collected for the Lockne structure.

The Lockne impact crater in central Sweden has features characterizing a relatively deep (several hundred meters) marine environment [3, 4]. Recently, improved outcrop has favored examination of important features, resulting in greater precision and understanding. The target sea-bed consisted of 80 m Cambrian and Ordovician, half lithified limestone, half soft claystone, resting on a peneplain cut into crystalline basement. The crater in the basement is just over 7 km wide. No raised crater rim is to be seen, but the crater is surrounded by a roughly 50 m thick brim of ejected crystalline rock, resting on the peneplain and some remaining sediment. Previous numerical modeling [2, 5] resulted in the most probable water depth estimate of 700 to 900 m at the time of impact. The water transport of ejecta has been proved as the main specific feature of the Lockne cratering ecent. Here we present some additional results of the 2D numerical modeling conducted to give more theoretical constraints for the geologic data interpretation and, in a respond, to control the numerical model assumption with the field observation.

Numerical Model: The SALEB numerical code has been used to compute the shock wave, transient crater growth, material ejection in a double layer target: a water layer of 700 to 1000 m over the granite basement. The sedimentary layer is computed as a granitic one with a simple separate tracing of particles initially situated in this thin (~80m) layer. ANEOS [7] equation of state is used to compile tabulated EOS for water and granite. Mechanical model for rocks includes brittle disruption in shear and tension, dry friction behavior of disrupted rocks, thermal softening close to the melting point (zero strength and friction for melts). To reproduce the complex morphology of impact craters with a central uplift the acoustic fluidization model is implemented [8].

The asteroid modeled as a granite sphere of ~500 m in diameter impact the see surface with the velocity of 15 km s^{-1}.

Preliminary results: Fig. 1 presents transient crater depth, diameter and volume for the first 40 seconds of the cratering process (parameters are measured in relation to the initial solid target surface.

The transient cavity in basement rocks grows approximately 15 seconds reaching maximum depth 1.8 km below the see floor level and a maximum volume of 15 km^3. Later the transient collapse begins and transient crater depth and volume decrease. The maximum transient crater diameter reaches~6.5 km measured at the pre-impact see floor level. The main ejection of the basement material takes approximately 20 to 25 seconds. The transient crater diameter after ejection is finished continue to grow due to the transient crater collapse.

The estimated volume of ejected material (all particles ever uplifted 200 or 300 meters above the pre-impact sea level) is ~ 6 km^3. This value corresponds to ~40% of the maximum transient crater volume.

The initial position of ejected crystalline rocks is shown in Fig. 2. The maximum excavation depth of rock material is about 600 m under the sea floor level. In comparison with this excavation depth estimate the presence of ~80 m of sediments does not change dramatically the general picture of cratering.

The total amount of impact melt in calculations is about 200 10^6 m^3. Overlapping black dots in Fig. 2 show the initial position of the ejected part of impact melt. The ejected melt volume is about 40 10^6 m^3, or 20% of the total melt volume. This material is incorporated in fragmented ejecta. The rest of impact melt cover the transient crater surface going up and down in a course of the crater collapse. The model does not include any mechanisms of melt interaction with water. Such an interaction possibly includes some local vapor explosions observed in volcanic lava flows entering see water.

Fig. 3 shows the calculated distribution of ejected rocks in respect to the maximum shocks pressure. The "average" shock loading level for ejected material is about 2 GPa. 50% of ejected rocks has experienced shock compression in the pressure range from 0.6 to 4 GPa (6 to 40 kbars). This is below the level of main microscopic shock metamorphism features like PDFs.

Only ~10 % of ejected rocks have been compressed above 10 GPa. The volume of ejected impact melt (~40 10^6 m^3) is about 0.7% of the total ejecta.

Due to the presence of water the main mass of ejecta cannot fly out far from the crater center. In the presented calculations only 0.5% of the total ejected volume has a chance to create distant ejecta (beyond the zone covered with the computation grid). The main part of ejecta is deposited through sea water moving outward and inward. To estimate the ejecta distribution one needs to take care about sedimentation rate for various fractions of clastic material. Here we make estimates of the first order accuracy - rocky material in our current model behaves as large (meter to ten meters or so) size blocks sinking in the water stream. Even for this simple model the redistribution of ejected material with a water stream is obvious enough. To get an impression about redistribution of ejected material by a water flow we estimate that, finally, ejected material is distributed in a circular zone of 7 to 8 km in radius (14 to 16 km in diameter). This radius is defined by the maximum water cavity radius.

The model predicts the thickest ejecta deposits just inside the crater rim (radial distance of 2 to 3 km). Close to the center and beyond the rim area the volume of ejected material is large enough to create the deposited layer with an effective thickness of 10 to 40 m. These estimates correspond to the uniform distribution of ejecta. Possible radial "rays" of ejecta may create thicker deposits in some radial direction at the expense of other directions. However, if one assume that rays cover 1/2 or 1/3 of the area, the thickness estimates should be multiplied by factor of 2 or 3 only. In addition one should mention that the possible presence of depressions/ridges at the initial see floor may affect the uniformity of ejecta distribution. In addition the water flow can carve channels in the pre-impact surface.

Conclusions: Despite a lot a factors which control the ejecta deposition in a sub-marine impact one can make some solid conclusions from the presented model:

- Ejected material is only slightly contaminated my impact melt. It is mostly rocky material shocked below 2 to 4 GPa of shock pressure.

- The main volume of ejecta is mixed with water at the inner side of the water transient crater. Hence the distance of 7 km from the center should be a distinct stratigraphic boundary: ejecta driven by a water flow cannot be deposited beyond this distance for the vertical impact. An oblique impact [2] should be assumed to explain possible presence of more distal ejecta.

Acknowledgements: The work is supported by Sweden Academy of Sciences.

References: [1] Lindström M. et al. (2003) In *Proc. of Mora Impact Woirkshop*, Elsevier, in press. [2] Shuvalov V. et al. (2003) In *Proc. of Mora Impact Woirkshop*, Elsevier, in press. [3] Lindström et al. (1996) *MAPS* 31: A80. [4] Sturkell E. (1998) Geol. Mag. 135: 121-127 . [5] Ormö J, Shuvalov V and Lindström M (2002) *JGR*, in press. [7] Thompson, S. L., Lauson, H. S. (1972) Sandia National Laboratory Report SC-RR-71 0714. [8] Melosh H. J., Ivanov B. A. (1999) *Annu. Rev. Earth Plant. Sci.*, 27, 385-415.

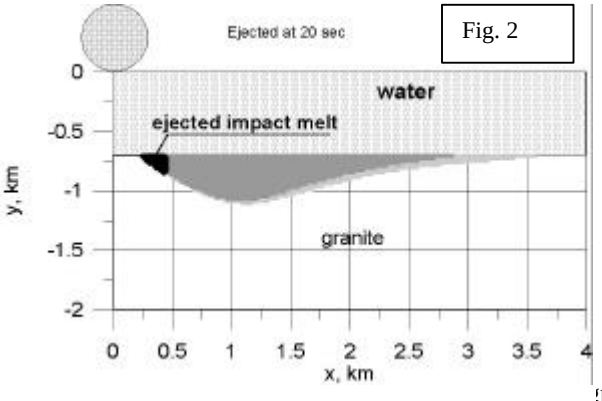

Fig. 2

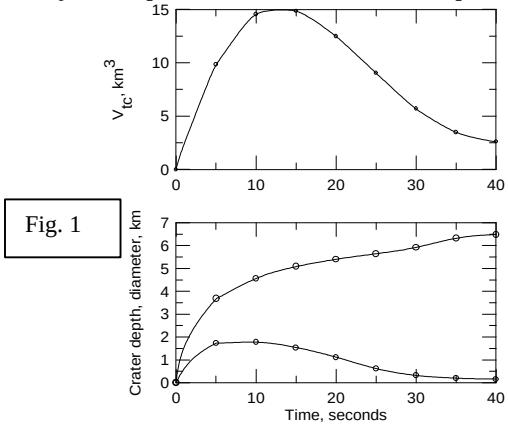

Fig. 1

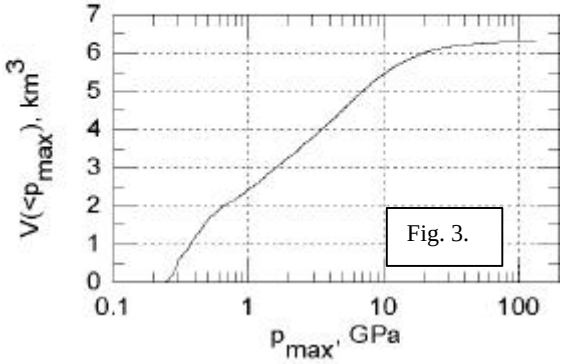

Fig. 3.

Fig. 3. Cumulative distribution of variously shocked ejecta.

SPINEL HETEROGENEITY WITHIN INDIVIDUAL IMPACT SPHERULES FROM THE K/T BOUNDARY: IMPLICATIONS FOR MODELLING OF IMPACT PLUME CONDITIONS.

A T Kearsley[1], G A Graham[2], A P Jones[3] and C R L Friend[4], [1] Electron Microscopy and Microprobe Analysis, Department of Mineralogy; The Natural History Museum, Cromwell Road, London SW7 5BD, UK, antk@nhm.ac.uk, [2] Lawrence Livermore National Laboratory, Livermore, California, USA, [3] Department of Earth Sciences, University College London, Gower Street, London WC1E 6BT, UK, [4] Department of Geology, Oxford Brookes University, Oxford OX3 0BP, UK.

Introduction: Minerals of the spinel group have been reported widely from sedimentary sequences that span the boundary between the Cretaceous and Paleogene Systems [1]. Distinctive nickel-bearing spinels are found associated with other evidence of global catastrophe due to major impact of an extraterrestrial body. Loose spinel grains can be easily extracted from soft sediment samples (e.g. deep sea sediment cores), and are readily concentrated by magnetic and density techniques. In many cases they show a dendritic morphology that suggests that they have grown rapidly [2]. Unfortunately, disaggregated samples usually do not preserve the textural relationship between spinel and other minerals, and may break fragile, complex grains into large numbers of skeletal fragments. As a consequence, it can be very difficult to determine the history of changing spinel composition that may reflect an evolving petrological environment.

Many authors have noted that there is a wide range of spinel compositions known from K/T boundary samples, with notable differences between geographical localities. Enrichment in nickel serves to distinguish these impact-related grains from detrital terrestrial grains. There has been considerable debate as to the environment and mode of growth for impact-related spinel, with some authors advocating location within an ablation-cloud generated during atmospheric entry of a large bolide [3] or condensation within an impact plume. Others have noted that remnants of the rare Fe^{2+}rich oxide magnesiowustite imply growth in a melt of ultrabasic composition under low oxygen fugacity [4]. Differences between types of petrogenetic setting may be recorded in the growth form of well-preserved spinels, for example in late Eocene spherules from Massignano, which have undergone partial diagenetic dissolution to reveal complex dendrites [2].

Spinel Composition: It appears that there is a substantial difference between the compositional range of K/T boundary spinels found in the Pacific Ocean core samples and the Atlantic area [1]. Recent models e.g. [5] have suggested that diverse chemistry may reflect evolution of composition, temperature and oxygen fugacity within a major impact plume during migration from the Chicxulub crater. Models of condensation predict that spinel composition should evolve from low-Mg, high-Fe^{2+} initial crystallisation to progressively more magnesian composition. This trend does fit within the diverse range of compositions reported from the 'Atlantic' area, although it does not seem to account for the Al-enrichment seen in the 'Pacific' area. Can well-preserved spinel textures and compositions verify the sequence of crystallization, and validate this model?

Spinels from Furlo, Italy: Spinels are common within the green and black spherules of the Furlo section in Italy [6]. Polished sections of the pale pink limestones beneath the red K/T boundary clay layer reveal burrows that contain transported spherules in varying states of diagenetic alteration. Some spinel-rich spherules show relatively little compaction, and preserve the relationship between spinel and the groundmass of phyllosilicates that have replaced glass and mafic minerals (figure 1). Fine outline shapes suggest co-tectic crystallization with mineral phases now altered or lost.

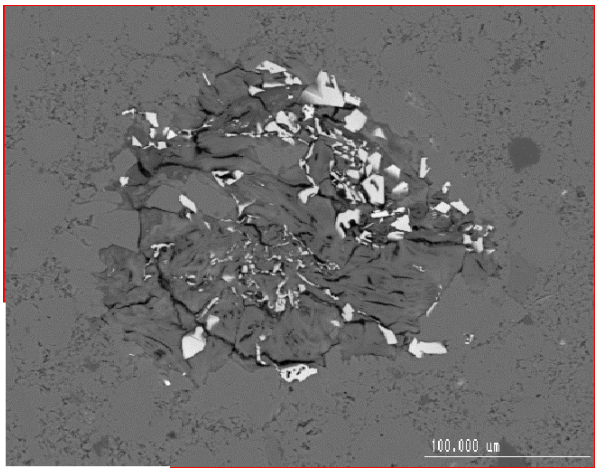

Figure 1. Backscattered electron image of a spherule, pale areas are spinels of diverse composition.

A sub-millimetre spherule may show dozens of spinel areas in cross section. The spinels may show evidence of outward growth from nuclei, and are often zoned with respect to their content of Mg, Al, Cr, Fe and Ni. Individual grain cross sections are so small as to be close to the limit for conventional electron probe microanalysis, but careful selection of areas that do not show substantial X-ray signal from the matrix does

yield good stoichiometric analyses (table 1). These may be of almost uniform composition, or can reveal a diversity that encompasses the entire range of the 'Atlantic' area within a single spherule (figure 2). Anhedral spinels within the spherule cores are often Mg and Al-rich, with a trend to Fe, Ni and Cr enrichment in coarser euhedral grains close to the spherule rim.

element	Centre	near edge	at edge
Si	1.08	0.07	0.44
Al	2.66	0.94	0.46
Cr	0.07	0.14	0.45
Fe3+	11.52	14.64	14.22
Ti	0.20	0.14	0.18
Mg	6.17	3.42	0.69
Fe2+	0.06	1.80	2.39
Mn	0.15	0.45	0.63
Co	0.11	0.11	0.14
Ni	1.21	1.78	2.10
Ca	0.23	0.43	2.01
'Divalents'	8.00	8.00	8.00
'Trivalents'	15.57	15.93	15.79
Total 'metals'	23.57	23.93	23.79

Table 1. Stoichiometric compositions of representative spinels from centre and edge of the spherule in figure 1. Formulae based on 32 oxygens, Fe^{3+} calculated from excess iron above 8 atoms in divalent total, checked by calculation of extra oxygen in analytical total.

Discussion: The zonation trend with regard to Mg : Fe^{2+} suggests that growth followed a compositional path akin to crystallisation during cooling of terrestrial basic melts (but with no strong association between Mg and Cr). This appears to be in the opposite direction to that predicted in condensation models. Unfortunately, in Furlo spherules, although spinel textures can be relatively well preserved, the extensive diagenetic alteration of silicate components prevents calculation of melt normative composition and consequent modeling of the crystallization sequence. Nor is there a simple explanation for higher aluminium contents in 'Pacific' spinels. Several important questions are raised. Do differing spinels within a single burrow suggest that the composition of individual melt droplets was diverse? Does this imply a highly heterogeneous impact plume? Could the spherules be derived from differing fine-scale mixes of target materials? Could the high aluminium content of the 'Pacific' spinels imply a very different melt composition? Could they even come from a different crater?

We suggest that careful in-situ analyses of spinels within spherules from worldwide locations may provide some of the answers to these questions and provide robust explanation of impact spinel petrogenesis.

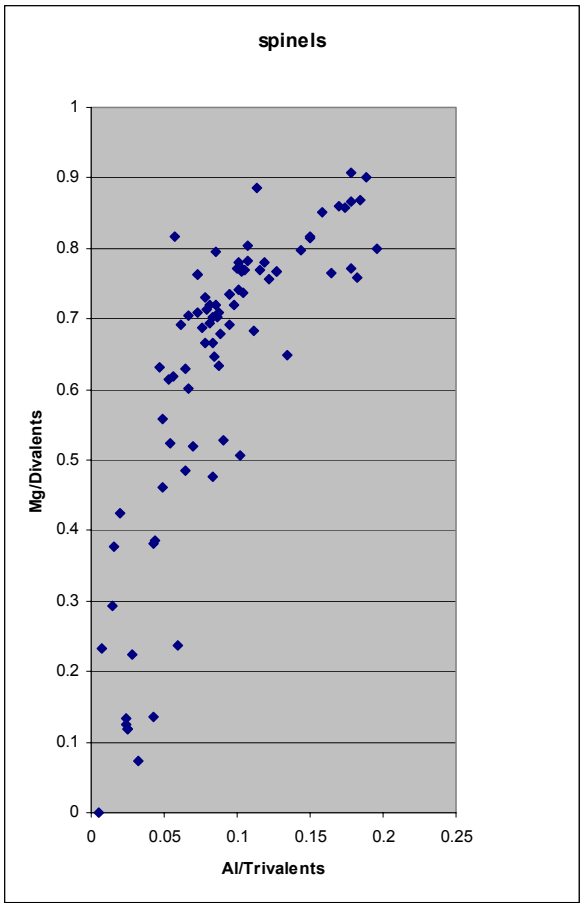

Figure 2. Plot of Mg/total divalent ions versus Al/total trivalent ions for the spinels in the spherule of figure 1. The plotted field is close to the entire range reported for spinels in the 'Atlantic' region.

Acknowledgements: we thank Sandro Montanari for his assistance in locating suitable samples in the field, Jon Wells for the preparation of the polished sections, and Oxford Brookes University for use of electron microprobe facilities.

References: [1] Kyte F T and Smit J (1986) *Geology, 14*, 485-487. [2] Kearsley A T and Graham G A (2002) *MAPS, 37.7,* A75. [3] Robin et al. (1992) *EPSL, 108*, 181-190. [4] Kyte F T and Bohor (1995) *GCA, 59,* 4967–4974. [5] Ebel D S and Grossman L (2001) *MAPS, 36.9,* A53 . [6] Montanari A and Koeberl C (2000) *Impact Stratigraphy: The Italian Record*, Lecture Notes in Earth Sciences, *93*.

CHICXULUB IMPACT PREDATES K-T BOUNDARY: SUPPORTS MULTIPLE IMPACT HYPOTHESIS G. Keller[1], W. Stinnesbeck[2], T. Adatte[3], D. Stüben & U. Kramar[4],[1]Department of Geosciences, Princeton University, Princeton NJ 08544, USA **gkeller@princeton.edu**, [2]Geological Institut University of Karlsruhe, D-76128 Karlsruhe, Germany, [3]Geological Institute, University of Neuchatel, 2007 Neuchatel, Switzerland, [4]Institut for Mineralogy and Geochemistry, University of Karlsruhe, D-76128 Karlsruhe, Germany.

Yaxcopoil 1, drilled on the inner flank of the transient cavity of the Chicxulub crater, was expected to yield the final proof that this impact occurred precisely 65 m.y. ago and caused the mass extinction at the Cretaceous-Tertiary (K-T) boundary. Instead, contrary evidence was uncovered. Biostratigraphic, sedimentologic and geochemical investigations reveal that the Chicxulub impact predates the K-T boundary by nearly 300 k.y. and did not cause the end-Cretaceous mass extinction.

The critical biostratigraphic evidence is in the tiny unicellular planktic foraminifera that lived in the upper water mass of the oceans during the late Maastrichtian and suffered extinction of all tropical and subtropical species at the K-T boundary 65 m.y. ago. In Yaxcopoil 1 a diverse late Maastrichtian species assemblage of these microfossils is present in a 55 cm thick bedded and laminated dolomitic mudstone that overlies the suevite impact breccia. The assemblage includes globotruncanids, rugoglobigerinids, heterohelicids, globigerinellids, hedbergellids and *Plummerita hantkeninoides*, the index species that marks zone CF1 and the last 300 k.y. of the Maastrichtian. This species assemblage was deposited in an open marine environment at about 150 m depth and under normal pelagic conditions (no significant reworking and transport of sediments). In contrast, sediments below the impact breccia were deposited in a shallow lagoonal environment that supported no planktic foraminifera.

Sediments also reveal normal open marine deposition after the impact event. The bedded and laminated dolomitic mudstones above the suevite breccia indicate normal deposition in a relatively quiet deeper water environment with occasional current activity (e.g. minor cross-bedding, 2cm-thick microconglom- erate). The 8 cm below the K-T boundary consist of bioturbated dark gray marly limestone containing an impoverished latest Maastrichtian planktic foraminiferal assemblage and burrows infilled with light gray early Danian sediments. Within these sediments occasional fragments of shallow water limestone and one glass fragment were observed. But there is no evidence of major reworking of the underlying breccia.

The K-T boundary is at the base of a 2 cm thick dark gray marly limestone containing mature glauconite. Above it are a 3 cm-thick flaser bedded and a 3 cm-thick mottled intervals, both containing diverse early Danian upper *P. eugubina* zone P1a(2) assemblages. The juxta-position of zone P1a(2) and late Maastrichtian zone CF1 indicates a major hiatus (200-300 k.y. missing) spanning the earliest Danian zones P0 and P1a(1) and probably the uppermost part of CF1. Another hiatus is present above the mottled interval at 7 cm above the K/T boundary where an upper zone P1c assemblage is juxtaposed over the zone Pla(2). The K-T boundary is thus missing and the early Danian is partially present.

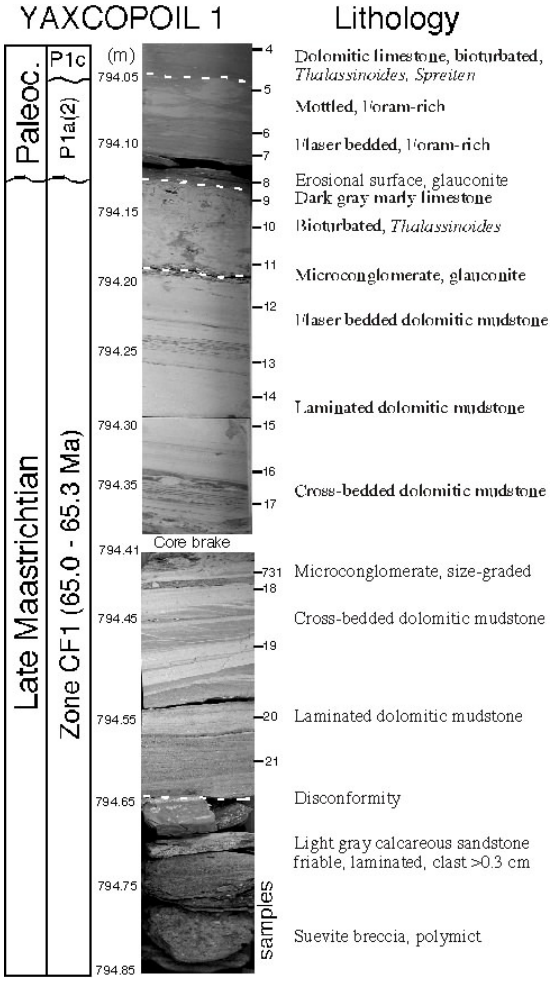

The lithologic, biostratigraphic and faunal analyses of Yaxcopoil 1 thus reveal a pre-K-T age for the Chicxulub impact. There are previous reports of a pre-K-T age for the Chicxulub impact based on earlier Yucatan drill cores [1, 2], and northeastern Mexico sections [3-6] and more recently the discovery of multiple impact spherule layers [7-9].

The age of the Chicxulub impact is estimated at 65.27± 0.03 Ma based on correlation with the oldest Chicxulub impact ejecta layer (microtektites) in northeastern Mexico [8-10]. The end of the Cretaceous thus experienced multiple impacts (comet shower?) rather than a single large impact as generally hypothesized. Chicxulub was one of these. Other smaller craters have recently been reported from the Ukraine (Boltysh) and North Sea (Silverpit)[11, 12]. In addition, Maastrichtian Ir and PGE anomalies have been reported form Oman and Israel [13, 14]. In addition, Ir anomlies have been reported from the early Danian in Haiti, Guatemala and Mexico [9]. Thus there is evidence for three impact events: late Maastrichtian, K-T boundary and early Danian.

The discovery of multiple impacts during the K-T transition fundamentally changes the current impact debate and refocuses attention on biotic and environmental effects of large impacts, the nature of the K-T mass extinction, whether gradual or sudden, and the effects of multiple impacts and major volcanism upon biota and in causing mass extinctions.

[1] Lopez-Ramos E. (l975) Plenum Press, N.Y. 257-282. [2] Ward W.C. et al. (l995) *Geology*, 23, 873-876. [3] Keller G. et al. (l994) *Palaios*, 9, 144-157. [4] Keller G. et al. (l997) *GSA Bull*. 109, 410-428. [5] Stinnesbeck W. et al. (l996) W. W. Norton & Co. p.471-518. [6] Adatte T. et al. (l996) *GSA Special Pub*. 307, 197-210. [7] Stinnesbeck W. et al. (2001) *Can J. Earth Sci.* 38, 229-238. [8] Keller G. et al. (2002) *GSA Special Pub*. 356, 145-161. [9] Keller G. et al. (2003) *Earth-Science Reviews* 1283, 1-37. [10] Stueben D. et al. (2002) *GSA Special Pub.* 356, 163-188. [11] Stewart S.A. and Allen P.J. (2002, *Nature* 418, 520-522. [12] Kelley P.S. and Gurov E. (2002), *Met. & Plan. Sci*. 37, 1031-1043. [13] Ellwood B.B. et al. (2003) *EPSL* 206, 529-540. [14]Adatte T. et al. in prep. [15] Li L. and Keller G. (l998) *Geology* 26, 995-998. [16] Courtillot V. (l999), Cambridge Univ. Press 147 p. [17] Hoffman C. et al. (2000) *EPSL* 180, 13-27. [18] Knight K.B. et al. (2003) *EPSL* 208, 85-99.

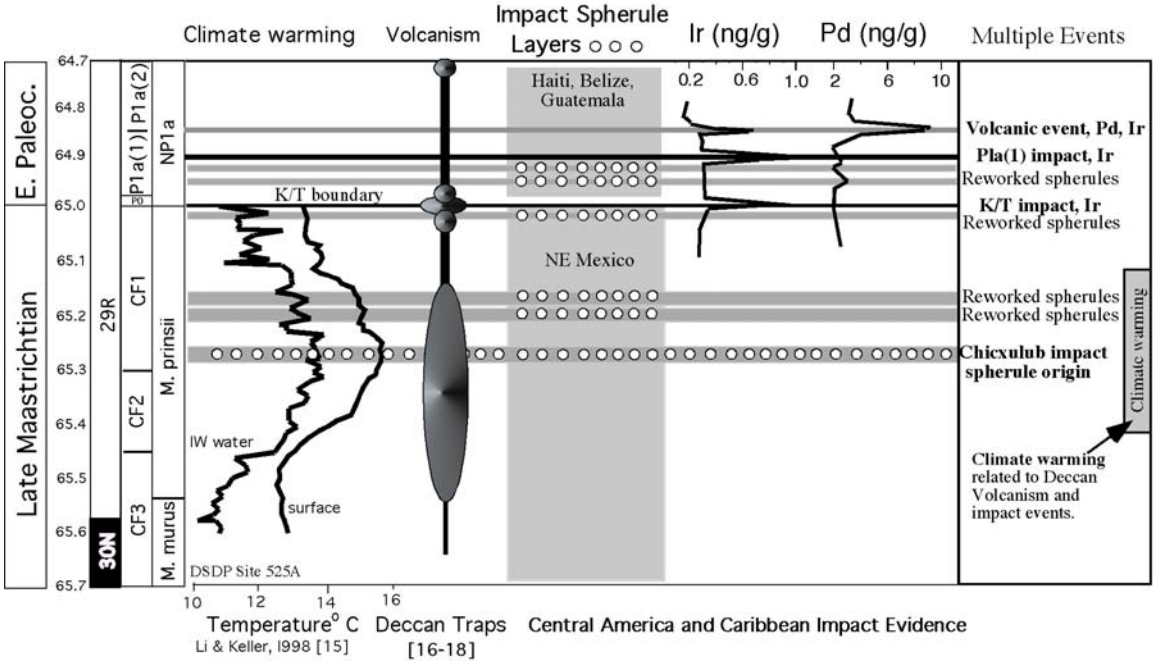

The Upheaval Dome impact crater, Utah: Combining structural and numerical data to constrain age, diameter, and amount of erosion. T. Kenkmann[1] and B. A. Ivanov[2], [1]Institut für Mineralogie, Museum für Naturkunde, Humboldt Universität Berlin, Invalidenstrasse 43, 10115 Berlin, Germany, thomas.kenkmann@rz.hu-berlin.de, [2]Institute for Dynamics of Geospheres, Russian Academy of Science, Moscow, 117939, Russia. baivanov@online.ru

Introduction: Upheaval Dome is located in southeastern Utah on the Colorado Plateau. The circular structure represents the remnant of a deeply eroded complex impact crater and provides spectacular insights into the architecture of a crater floor. By combining structural and numerical data we try to constrain the structure in time and space.

Pressure estimates: Shatter cones in sandstones of Moenkopi Formation described by [1] are not fully developed and partly ambiguous. Sets of subplanar microstructures in quartz of the White Rim Sandstone, documented by [1] and [2] are frequent and most commonly represent planar fractures. Up to date we failed to present PDFs with SEM and TEM. This suggests that the presently exposed rocks were affected only by a strongly attenuated shock or pressure wave, most likely below 5 GPa. We found a method to define a lower pressure limit more precisely for the rocks of the innermost part of the central uplift, based on the recognition of deformation mechanisms [3] that are experimentally calibrated with respect to pressure:

The complex occurrence and geometry of the White Rim Sandstone (Fig.1) indicates an almost complete loss of internal coherence during deformation. The sandstone displays extreme thickness variations, blind terminations and frequent embranchments at nodular-like points. This, together with discordant contacts to the country rock, shows that the sandstone builds up a network of dykes that were emplaced and injected during formation of the central rise. Micro-

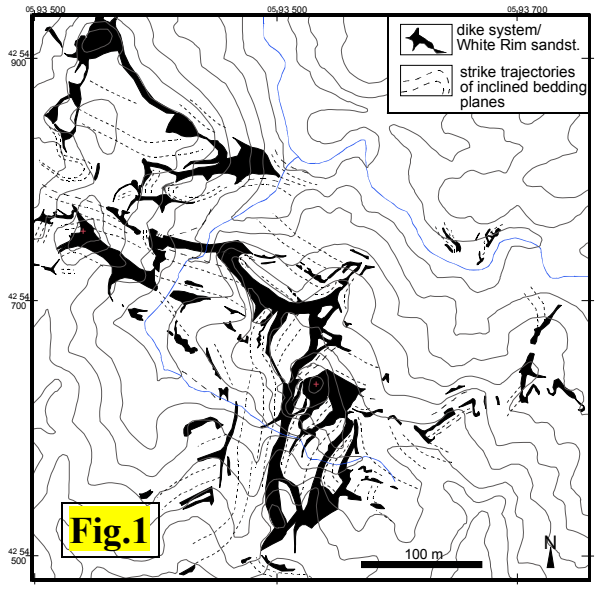

structural analyses revealed that the macroscopically ductile appearance is achieved by distributed cataclastic flow. Beside inter- and intragranular fracturing, dislocation pile-ups, dislocation arrays and tangles indicate additional dislocation glide activity in quartz of the White Rim Sandstone during deformation. The undeformed White Rim Sandstone is pure in composition, has a grain size of 140 µm, and a porosity of 19 %. The distributed cataclastic flow was initiated by grain crushing, collapse of pore space, and subsequent intergranular shear. The grain size of the deformed sandstone is 46 µm and contains >40 % comminuted matrix and minor porosity. In accordance to experimental data for a very similar sandstone (Berea sandstone)[4] it is suggested that a high effective confining pressures, in excess of 250 MPa was necessary to cause this flow. At shallow crustal levels (the maximum possible depth of burial of the White Rim Sandstone on the Colorado Plateau is 3 km, corresponding to ~80 MPa) such a high confining pressure cannot be realized by the lithostatic overburden. However, this pressure can be built up transiently by an attenuated pressure pulses during an impact process.

We can conclude: At the present depth below the crater the shock wave attenuated to magnitudes below the Hugoniot elastic limit of quartz but was still well above any possible lithostatic pressure of this region.

Other structural constraints: Triassic and Jurassic layers of the crater display a strata thickening towards the center of the dome and a strata thinning towards its rim (Fig.2). They are a consequence of convergent inward flow during crater collapse. The systematic change in thickness obeys a power law function of the form: $h/h_0 = A\,R^y$, with h being the thickness of a layer at a radius R from the impact center, h_0 being the initial layer thickness, and y being a power law factor. The amount of thickening increases from footwall to hangingwall units. Geological cross sections constructed across Upheaval Dome show that the distance of the axis of the ring syncline to the center of the structure increases from footwall to hangingwall units from 1.4-1.5 km (Moenkopi F.) to 1.7-1.8 km (Navajo sandstone) in both NNE-SSW and WNW-ESE profiles.

Fitting a numerical model to the structure: Our pressure estimates and the above mentioned structural features represent the frame numerical models have to be fitted to. Using the 2-dimensional multimaterial Eulerian SALE-B code we simulate the crater formation due to a vertical impact of a spherical asteroid

500 m in diameter with the velocity of 12 km s^{-1}. According to a standard scaling law the impact should produce a complex crater ~7 km in diameter. The mechanical model includes brittle damage, thermal softening and acoustic fluidization of the target [4]. The model allow us to record initial shock compression and the following rock displacement. Fig. 3 demonstrates the final geometry of initially flat strata in the target.

The model shows that in order to achieve a shock compression below 5 GPa in the presently exposed rocks, the Permian-Triassic boundary (white and red strata in Fig. 4) has to be ~2 km below the ancient surface when the bolide struck the Earth. A radius distance of the ring syncline axis of 1.4-1.8 km as observed at Upheaval Dome is found to occur at a depth of 1.6-2.0 km in the best fitted model (Fig. 3).

The strongest increase in layer thickness toward the center of the structure occurs in the numerical model at a depth of 2.075 km (Fig. 2). However, this increase is limited to the immediate vicinity of the center of the structure (below 500 m), in contrast to Upheaval Dome, where an increase in layer thickness is already observed at 1-2 km, pending on the layer. The reason for this discrepancy is not yet clear to us but may depend on the rheological input parameters of the model.

Combining model and observation, the White Rim Sandstone (Uppermost Permian) was at a burial depth of ~2 km when the impact occurred at Cretaceous times during deposition of the Mancos shales (most likely the Emery Sandst. Member). The initial diameter of the Upheaval Dome impact was about 7.5 km.

Acknowledgement: This work is funded by the German Science Foundation, grant KE-732-6. The von Humboldt prize makes this work possible for BAI. We are grateful to D. Scherler and A. Jahn for their help.

References: [1] Kriens, B. J. et al. (1999) *JGR, 104,* 18867-18887. [2] Kenkmann, T. and Scherler, D. (2002). *LPS XXXIII,* Abstract #1037. [3] Kenkmann, T. (2003) *EPSL* (submitted) [4] Menéndez et al. (1996) *J. Struct. Geol.,* 18, 1-16. [4] Melosh H. J., Ivanov B. A. (1999), *Ann. Rev. Earth Plant. Sci.*, 27, 385-415.

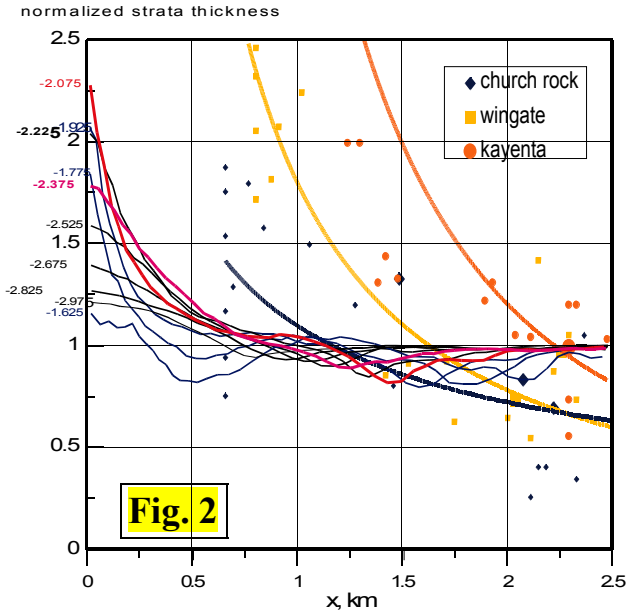

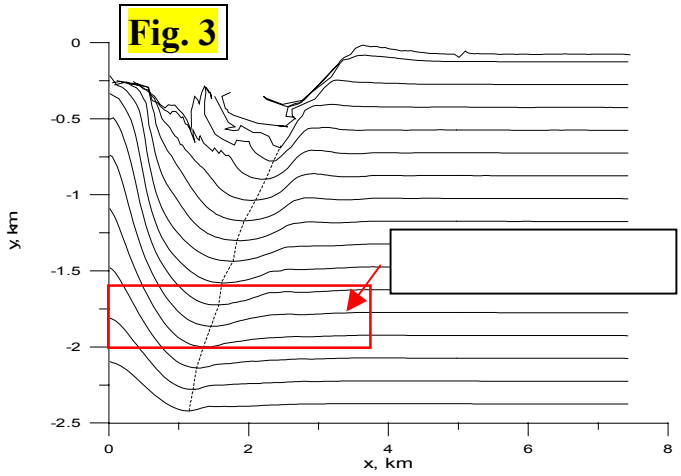

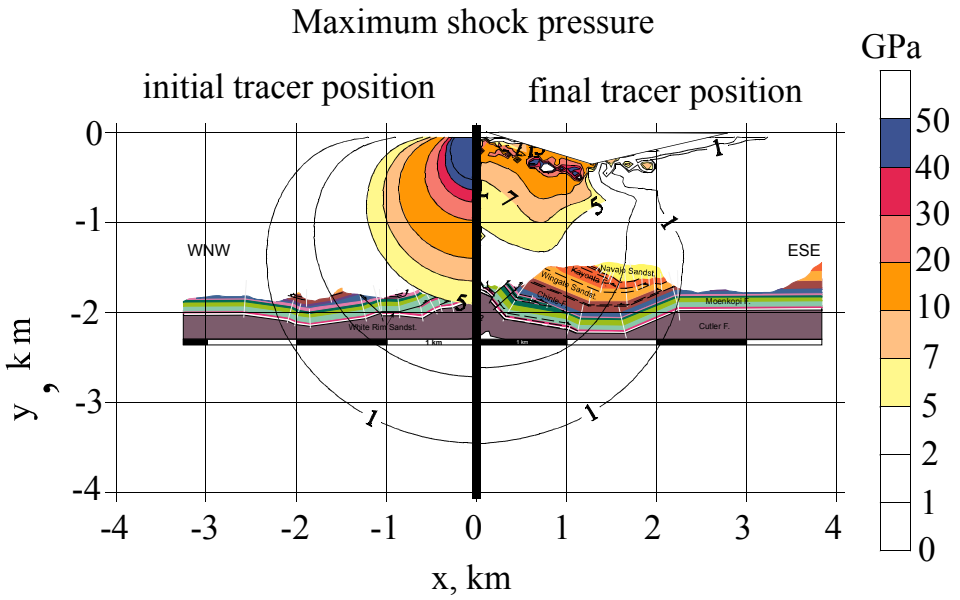

Fig. 4

The Cretaceous sequence of the Chicxulub YAX-1 drillcore: What is impact-derived? T. Kenkmann, A. Wittmann, D. Scherler, D. Stöffler, Institut für Mineralogie, Museum für Naturkunde, Humboldt Universität Berlin, Invalidenstrasse 43, 10115 Berlin, Germany, thomas.kenkmann@rz.hu-berlin.de,

Introduction: The Yaxcopoil-1 (Yax-1) borehole was drilled 60 km SSW of the center of the Chicxulub impact crater within the annular trough between peak ring and crater rim down to a depth of 1510 m. After penetrating 795 m of post-impact sediments of Tertiary age, about 100 m of suevites and melts and 615 m of Cretaceous sediments were recovered. The Cretaceous rocks consist of dolomites, limestones, and anhydrites, the latter representing 29-30% of the sequence. The age of the sequence is constrained at two levels: (1) at 1495-1455 m, where planktic foraminifers can be correlated with the Bonarelli event near the Cenomanian-Turonian boundary [1] and near the top of the sequence, where a Maastrichtian age was derived [1].

Deformation of the sequence: Stinnesbeck et al. [1] suggest that the Cretaceous sediments are undeformed, autochthonous, and comparable to Cretaceous sequences outside the crater. Brecciated units and clastic dikes (pers. comm) are explained to be of intraformational origin (solution collapse breccia). The authors state to have not found any indication for major disruption, mechanical fragmentation, shock alteration, and the presence of impact melt rock throughout the sequence, except for the suevite dikes. We disagree with these statements based on the following observations:

Shock metamorphism: Beside intense shock metamorphism at 909 and 916 m, several quartz grains in the paraconglomerate at 1036,52 m show PDF lamellae (decorated and nondecorated) in up to three directions (Fig.1a). These grains where found along a thin dark colored vein (Fig. 1b).

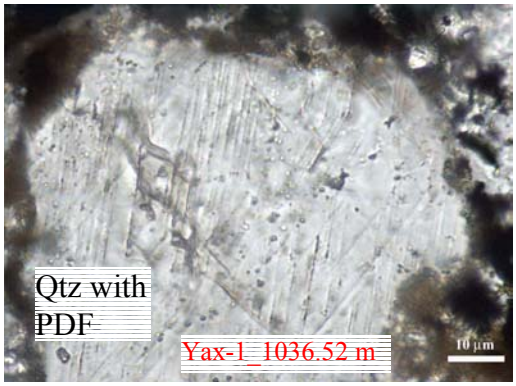

Fig. 1a

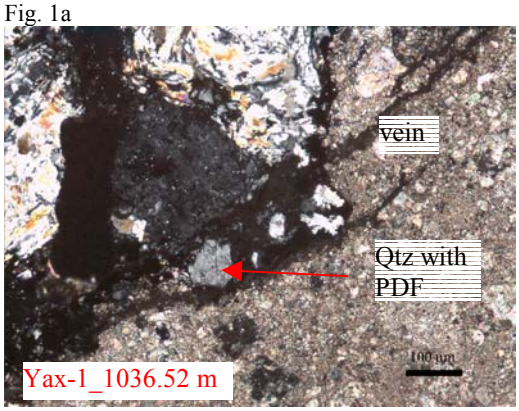

Fig. 1b

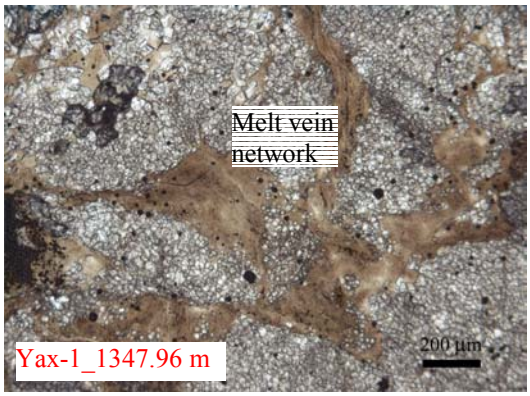

Fig. 2a

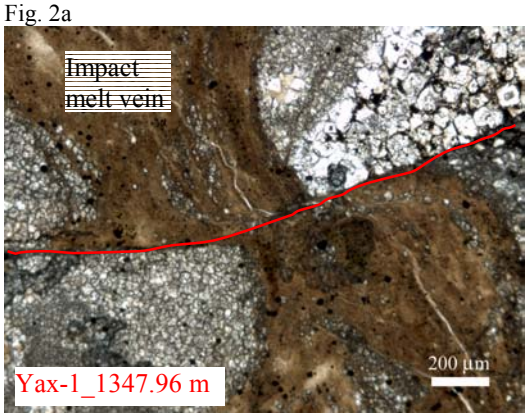

Fig. 2b

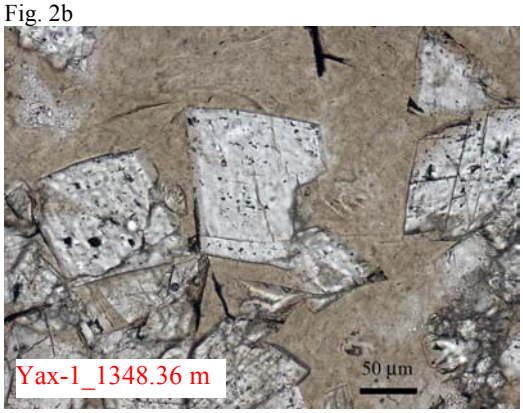

Fig.2c

Impact-melt rock: Devitrified melt rock of siliceous composition form anastomozing vein networks at 1347,9 m (Fig.2a). Their brownish color is due to the growth of clay minerals. The melt also occurs interstitially between dolomite crystals (Fig. 2c). Such interstitial fillings occasionally occur in the adjacent brecciated dolomites and are traceable down to 1368 m.

Clastic polymict dikes: According to [3] there are several polymict clastic dikes at a depth interval of 1300-1400 m cutting the stratification. Although exotic fragments such as crystalline rocks have not been discovered so far, a variety of at least 8-10 different lithologies which include lithic types that have not been observed anywhere else in the drill core, clearly demonstrate the polymictic nature of the dikes.

Tilting: We found that the scattering of bedding inclination is caused by (a) a non-horizontal deposition of sediments [2], (b) local solution phenomena and (c) the formation of chickenwire structures. However, the different mean inclination in certain depth intervals (Fig. 3) can not be explained by this process and may indicate a mechanical decoupling at ~916 m and at 1315-1410 m.

Stratigraphy: A stratigraphic continuity of a 615 m thick column cannot be ruled out as proposed by [1] on the base of two biostratigraphic marker horizons. A comparison of Yax-1 with profiles outside the crater (T1, Y2, Y1, Y5, Y4) [4] shows that the fossil-rich units E and F [4] of Turonian-Santonian age are obviously lacking at Yax-1. The brecciated dolomites and anhydrites may probably correlate with unit G of [4]. Since a sedimentary hiatus is very unlikely in the view of continuous sections outside the crater, impact-induced detachments and displacements are favored.

Faulting: Faults near polymict clastic dikes formed cogenetically with the dikes [3]. Faults and fault breccias are associated with a strong grain size reduction and comminution along fault planes. This requires a higher effective confining pressure than would be expected in a solution-collapse scenario at subsurface levels. Faults also displace the impact melt veins (Fig. 2b) pointing towards a formation time after the injection of the melt veins. However, the sheared impact melt reacts viscously and this indicates a limited time hiatus between both events. Intraformational solution-collapse breccias may be present at 990-1000m, where large voids (partly filled with cements) occur. Otherwise, there is no evidence that anhydrite was dissolved. Anhydrite layers are fresh and anhydrite fragments are incorporated into the dikes. Brittle fault zones cut through anhydrite layers and nodules (Fig. 4). Large anhydrite crystals are cataclastically deformed and weakly sealed afterwards. This also indicates that faults are not caused by solution of anhydrite.

Preliminary kinematic model: Most likely the Cretaceous rocks were originally located outside the 90 km wide transient crater cavity (~65-70 km away from the point of impact) where a ubiquitous shock metamorphic overprint is not to be expected. They successively moved inward and downward during crater collapse. The suevitic dikes were probably injected from the ground surged suevite by a drag and spallation induced delamination of the uppermost Cretaceous sediments. The impact melt dike has formed at an early stage of cratering. The majority of breccias, faults and clastic dike formed during growth of the crater cavity and eventually during crater collapse.

Acknowledgement: This work is funded by the German Science Foundation (DFG), grant KE-732-8.

References: [1] Stinnesbeck et al. (2003). *Geophys. Res. Abstracts, 5*, 10868 [2] Kenkmann, T. et al. (2003). *LPS 34,* Abstract 1368. [3] Wittmann, A. et al. (2003). *LPS 34*, Abstract 1386.[4] Ward, W. C. et al (1995) *Geology*, 23, 873-876.

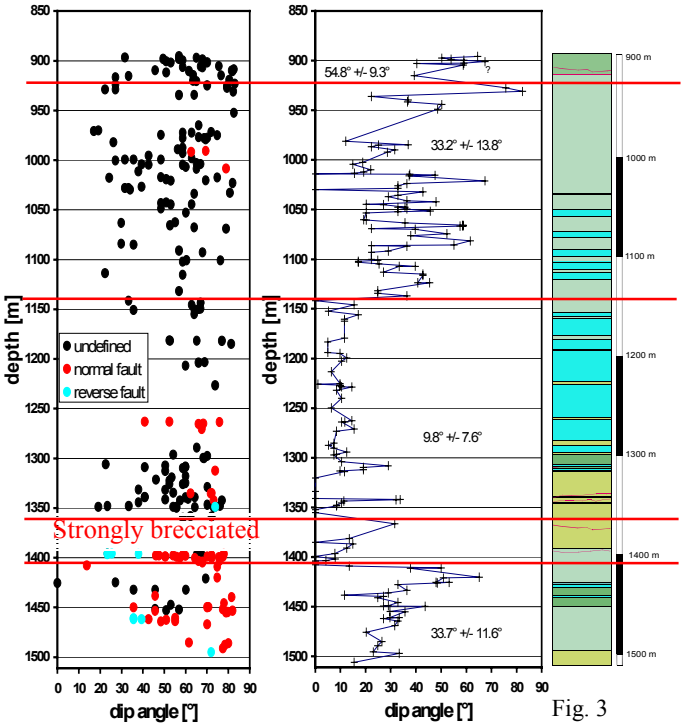

Fig. 3

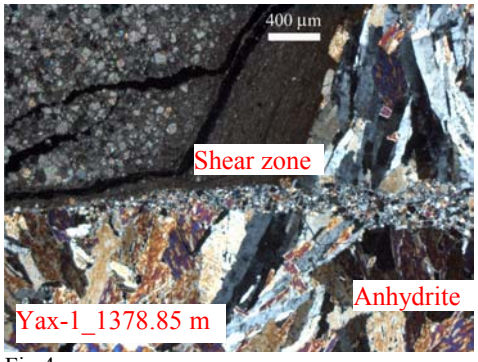

Fig.4

POSSIBLE MODES OF EMPLACEMENT OF COARSE IMPACTOCLASTIC EJECTA (BRECCIA) FROM A LARGE BODY IMPACT ON EARTH: CHICXULUB EJECTA IN BELIZE, CENTRAL AMERICA. D. T. King, Jr.[1], L. W. Petruny[2], K. O. Pope[3], and A. C. Ocampo[4], [1]Dept. Geology, Auburn University, Auburn, AL 36849-5305 [kingdat@auburn.edu], [2]Astra-Terra Research, Auburn, AL 36831-3323 [lpetruny@att.net], [3]Geo Eco Arc Research, 16305 St. Mary's Church Road, Aquasco, MD 20608 [kpope@starband.net], [4]ESTEC Planetary Division, European Space Agency, SCI-SB, Keplerlann 1, Noordwijk, The Netherlands [Adriana.Ocampo@rssd.esa.int].

Introduction: The Albion impactoclastic breccia [1], also called the Albion diamictite bed [2], which crops out on Albion Island, Belize (Figure 1), and nearby areas in Quintana Roo, México, is a very coarse, carbonate clast-rich unit that was formed by ballistic sedimentation and ejecta debris-flow processes in the aftermath of the large-body impact event approximately 325 km away at Chicxulub on the Yucatán Peninsula of México.

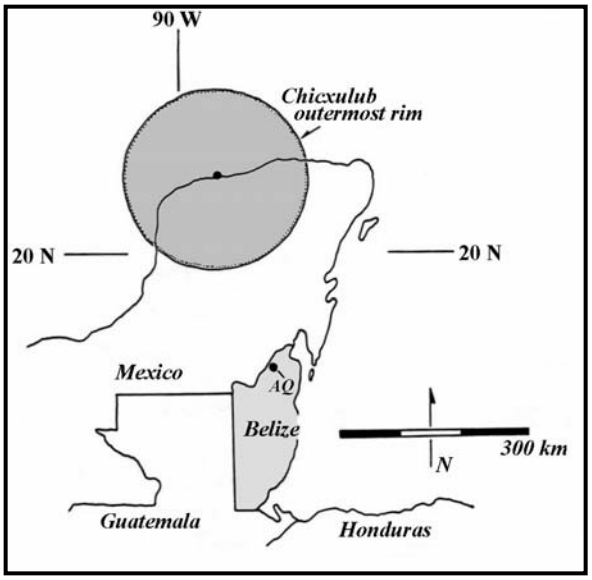

Figure 1. Location of Albion Quarry, Belize.

Stratigraphic relations: The Albion impactoclastic breccia (~15 m) is underlain by a ~ 1-2 m-thick, fine-grained impactoclastic unit containing accretionary lapilli and clay clasts (named also the Albion spheroid bed [2]). This finer grained unit underlies the impactoclastic breccia and together these two impactoclastic units comprise a mappable, isochronous, unconformity-bounded stratigraphic interval between upper Maastrichtian dolostones and lower Tertiary thin-bedded limestones in the study area [2].

Sedimentologic characteristics: In-situ grain-size counts reveal that the Albion impactoclastic breccias are generally extremely poorly sorted and have very high matrix content (< 1 cm or < -3.5 phi), which ranges from 60 to 85 percent. The mean size of stratigraphic levels either falls within the matrix (< 1 cm or < -3.5 phi) or is less than 5 cm (~ -5.6 phi. Where present, rather rare coarse boulders and fine blocks (i.e., size range 1 to 9 m or -10 to -13.3 phi) tend to strongly affect mean size (Figure 2). There is a dearth of observed grain sizes of clasts in the impactoclastic breccia for sizes between 30 cm and 1 m (-8.5 and -10 phi). There is a statistical indication of mixing of at least two distinct size populations within this impactoclastic breccia, and there is a general fining upward trend among stratigraphic levels studied at Albion Island [3].

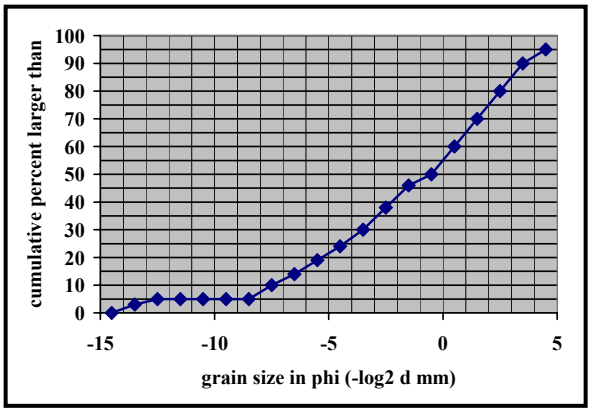

Figure 2. Typical cumulative grain-size frequency curve for the Albion impactoclastic breccia. Graph is based upon data from in-situ area counts for grains between -3.5 and -8.5 phi, microscopic area estimates for grains under -3.5 phi, and photographic area estimates for grains over -8.5 phi.

Transport history: Intensive comminution of grains, surface markings showing violent grain interactions, coated clasts and boulders, and internal fracturing of clasts are evidence of early turbulent interaction among debris in the collapsing Chicxulub ejecta curtain. However, flow laminations and flow-produced pseudo-bedding contacts, aligned platy clasts, and intact highly fractured clasts (i.e., clasts with 'jigsaw cracks') are evidence of subsequent, laminar or more

regular flow conditions within the impactoclastic breccia.

One possible explanation for the two clast populations and observed flow characteristics suggests mixing of ballistically transported (allochthonous) sedimentary material with locally derived (autothonous) boulders and blocks derived from secondary cratering. Alternatively, the mixing may derive from ejecta curtain interactions with the atmosphere and subsequent sorting of clasts into distinct flows that mix in the latter stages of deposition [4].

References: [1] Terminology of Stöffler D. and Grieve R. A. F. (1994) *LPS XXV,* 1347–1348. [2] Ocampo A. C. et al. (1996) *Geol. Soc. Amer. Spec. Paper 307,* 75-88. [3] King, Jr. D. T. and Petruny L. W. (2003) *Impact markers in the stratigraphic record*: Springer-Verlag, p. 203-227. [4] Pope, K.O. et al. (1999) *Earth Planet. Sci. Let., 170,* 351-364.

Proposed Scientific Drilling at the Bosumtwi Impact Structure, Ghana, West Africa. C. Koeberl[1], B. Milkereit[2], J. Overpeck[3] and C. Scholz[4], [1]University of Vienna, Austria, [2]University of Toronto, Dept. of Physics, 60 St. George St., Toronto, Canada, M5S 1A7, bm@physics.utoronto.ca, [3]ISPE, Tuscon, USA, [4]University of Syracuse, USA.

Introduction: The 10.5 km diameter Bosumtwi impact crater in Ghana (Fig. 1) is almost completely filled by Lake Bosumtwi. The crater has an age of 1.07 Ma and was excavated in lower greenschist facies metasediments of the 2.1-2.2 Ga Birimian Supergroup. The Ivory Coast tektites and microtektites originated from this crater [1]. A first high-resolution aerogeophysical survey was conducted in early 1997. Since then several projects have dealt with land- and lake-based geophysical measurements and surface geological and geochemical investigations regarding the subsurface topography of the structure [2] [3]. The results from these studies provided all the background work necessary to characterize the subsurface structure of the Bosumtwi crater that are necessary to define the targets for a deep drilling program. Such a deep drilling project, proposed by the authors, has recently been approved by the International Continental Scientific Drilling Program (ICDP). Drilling is desirable for several reasons, including 1) to obtain a complete 1 million year paleoenvironmental record in an area for which so far only limited data exist; 2) to study the subsurface structure and crater fill of one of the best preserved large young impact structures. Understanding the full range of climate variability in this region over the last 1Ma will thus fill a major hole in our understanding of global climate dynamics, and thus also lead to an enhanced climate prediction capability over a broad part of the earth. In terms of cratering studies, Bosumtwi is one of only two known young craters of this size, and may have a crucial diameter at the changeover between a traditional "complex" crater with a central peak and a crater structure that has a central peak-ring system.

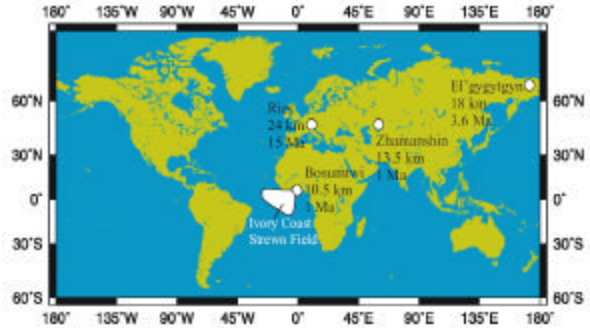

Fig. 1. Location of the Lake Bosumtwi Crater, the Ivory Coast strewn field, and comparable impact structures.

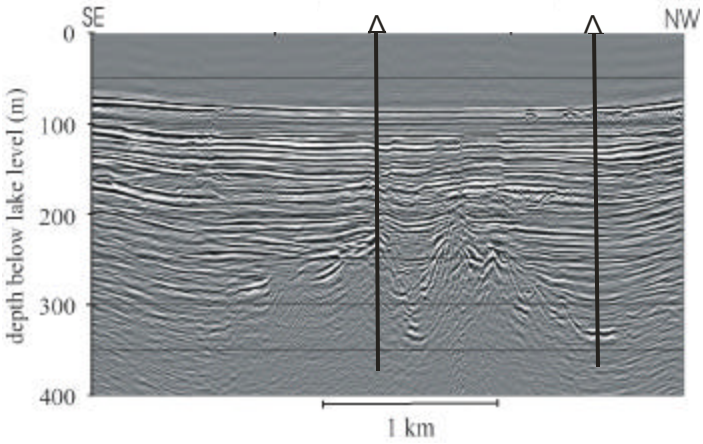

Fig. 2: Reflection seismic profile with central uplift and two proposed borehole locations [2]

References: [1] Koeberl, C. et al. (1997) Geochemica et Cosmochemica Acta, 62, 1745-1772. [2] Scholz, C., Karp, T., Brooks, K., Milkereit, B., Amoako, P., Arko, J., Lezzar, K. (2002) Geology, 30, 939-942. [3] Karp, T., Milkereit, B., Janle, P., Danuor, S., Pohl, J., Berckhemer, H., Scholz, C. (2002) Planetary and Space Science, 50, 735-743.

A 2003 EXPEDITION INTO THE LIBYAN DESERT GLASS STREWN FIELD, GREAT SAND SEA, WESTERN EGYPT. Christian Koeberl[1], Michael R. Rampino[2], Dona A. Jalufka[1], and Deborah H. Winiarski[2]. [1]Department of Geological Sciences, University of Vienna, Althanstrasse 14, Vienna, A-1090, Austria, (christian.koeberl@univie.ac.at), [2]Earth & Environmental Science Program, New York University, 100 Washington Square East, New York, NY 10003, USA (mrr1@nyu.edu).

Introduction: Libyan Desert Glass (LDG) is an enigmatic type of natural glass that is found in an area with an extension of several thousand square kilometers. Literature values on the extent vary between about 2000 and 6500 km². This area, or strewn field, is located between sand dunes of the southwestern corner of the Great Sand Sea in western Egypt, near the border to Libya. Therefore, the name "Libyan" Desert Glass is not entirely correct, given today's geographical boundaries, but refers to the traditional name of the desert. P.A. Clayton was the first to travel the region in the early 1930s and to collect glass samples that were used to provide the first detailed scientific description of the glass and its occurrence. In addition, R. A. Bagnold visited the LDG area in the 1930s. The inaccessibility of the LDG area was the reason for a relative paucity of visits to the location. In the 1970, visits by, for example, J.R. Underwood, E. P. Fisk, and V.E. Barnes led to the collection of a large number of LDG samples and some petrographical work [1]. In addition, two impact structures were discovered just west of the LDG strewn field, just over the border in Libya: the B.P. and the Oasis impact structures, which are of interest because of a possible connection with the origin of the LDG; see below for a more detailed discussion.

Petrography and Geochemistry: In macroscopic examination, the glass shows irregular shapes with signs of sand abrasion and other erosion features. The fission track age of LDG has been determined to be about 29 Ma (e.g., [2]). LDG is a very silica-rich natural glass with about 96.5-99 wt.% SiO_2, and shows a limited variation in major and trace element abundances. So far rather few trace element studies of LDG exist, but the available data (for example, those for the rare earth elements) indicate abundances and interelement ratios that are typical for upper crustal rocks. Libyan Desert Glass has, since its discovery, been the subject of a number of studies, ranging from glass technological aspects to petrographical and geochemical work.

The origin of LDG has been the subject of a controversy (see, e.g., [1, 3]), which - in the view of some researchers - is still not settled. However, the majority of workers favor an origin by impact (see, e.g., papers in [3]). There are, however, some differences to "classical" impact glasses, which occur in most cases directly at or within an impact crater. Evidence for an impact origin includes the presence of schlieren and partly digested mineral phases, lechatelierite (a high-temperature mineral melt of quartz), and baddeleyite, a high-temperature breakdown product of zircon.

The rare earth element abundance patterns are indicative of a sedimentary precursor rock, and the trace element abundances and ratios are in agreement with an upper crustal source. There is a similarity between LDG major and trace element abundances and Sr and Nd isotopic compositions and the respective values for rocks from the B.P. and Oasis impact structures in eastern Libya, but lack of age information for the two Libyan structures precludes a definitive conclusion. There are some good indications for the presence of a meteoritic component in LDG (e.g., [4]). Os abundances and isotopic values conform the presence of a meteoritic component in LDG [5]. This observation is difficult to reconcile with an airburst model, because it requires physical mixing between meteoritic and crustal matter in liquid form (i.e., in a melt phase).

Fig. 1. Systematic search in the LDG area for glass samples.

2003 Expedition: To obtain a better understanding of the distribution of the LDG in the strewn field, to search for possible impact-related breccias in the LDG strewn field, and especially to obtain further samples with dark streaks to better and more thoroughly study the meteoritic component, we undertook a 10-day expedition into the LDG area in early 2003. During systematic searches (which also helped to obtain information on the spatial distribution of the samples; Fig. 1), a large number of LDG was found (Fig. 2, 3). About 50 kg of LDG

samples, ranging up to 2.5 kg in weight, were collected, including about two dozen specimens with dark zones, layers, or generally dark appearance. There is a large variation in color and opacity of the various LDG samples. The larger ones are usually white/cloudy and not transparent, whereas some up to 10-cm-sized samples are clear and almost of gem quality (e.g., Fig. 4). A few samples were found to contain also other types of dark inclusions. The study of these samples is in progress and will be reported on separately.

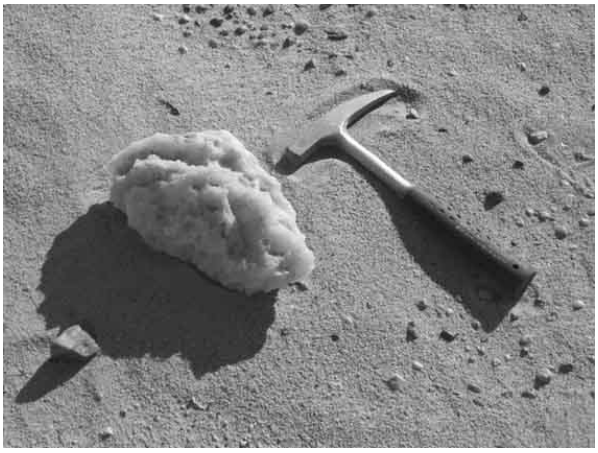

Fig. 2. One of the larger pieces of LDG recovered during the 2003 field trip.

Fig. 3. In some of the corridors between sand dunes in the LDG area, accumulations of several large specimens of different color and opacity were encountered.

Acknowledgment: CK is supported by the Austrian Science Foundation (project Y58-GEO).

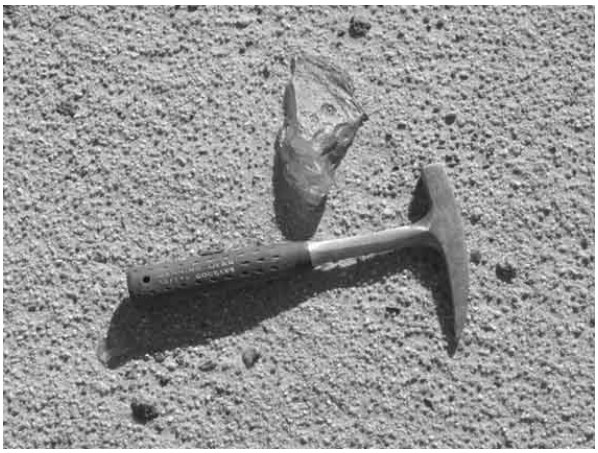

Fig. 4. A large, almost transparent LDG specimen. This samples also shows a dark layer that may contain a meteoritic component.

References: [1] Barnes V.E. and Underwood J.R. (1976) *Earth Planet. Sci. Lett.* 30, 117-122. [2] Bigazzi G and de Michele V (1996) *Meteoritics Planet. Sci.* 31, 234-236. [3] de Michele V. (ed.) (1997) Proceedings, Silica '96, Meeting on Libyan Desert Glass and related desert events. Pyramids Publ., Milan, Italy. [4] Barrat J.A. et al. (1997) *Geochim. Cosmochim. Acta* 61, 1953-1959. [5] Koeberl C. (2000) *Meteoritics Planet. Sci.* 35, A89-A90.

COLLAPSES AND DEPRESSIONS POST-DATING CRATER FORMATION IN MARTIAN IMPACT STRUCTURES – DISTRIBUTION AND CONSEQUENCES. J. Korteniemi, University of Oulu (Department of Physics / Division of Astronomy, P.O. Box 3000, Fin-90014 University of Oulu, Finland; jarmo.korteniemi@oulu.fi).

Introduction: The surface of Mars, especially the southern highlands, is saturated with impact craters. These structures display a variety of types, such as rampart, polygonal and double ring craters. This may depend on on the local geological environment at the time of the impact and after it [1].

Craters with distinctive depressions on their floors are found around the planet. The pits, collapses and depressions in such craters have clearly formed after the initial formation of the "parent" crater, and they seem to be unrelated to the crater age. Some of the depressions follow the circular crater shape., and almost none of them breach the crater rim. Thus they are clearly related to the crater structure and definitely not random. This study gives an overview on the distribution of the craters in question. It also classifies them into subtypes, and tests and suggests possible causes for the particular phenomenae involved.

Materials and methods: The primary materials for this study were the Viking MDIM2 digital image mosaics provided by the USGS [2]. The MDIMs, with a resolution of 256 meters per pixel, were used to locate and map out the craters around the planet and their distribution in specific areas. MDIMs were used to recognize different types of depressions, and to classify them into reasonable subtypes according to their size, shape, location and context. Geological mapping of various examples of the different types were made based on these mosaics.

Mars Global Surveyor MOLA altimetry data [3] was later combined with the Viking data. This was done to estimate the volume of the collapse. Secondly, the dimensions of the depressions were defined and slope angles calculated.

MGS MOC narrow angle images [4] were used to search for possible layers in the depression walls, in order to find clues for their formation processes. For this purpose, also Mars Odyssey THEMIS-VIS [5] and -IR nighttime images [6] were used. The THEMIS-IR daytime and MOC WA data sets were taken into the account in areas where the Viking images were either poor or inconclusive.

Only craters over 30 km or more in diameter were included in this study due to the resolution limitations of the MDIMs and MOLA data.

Preliminary results: The craters with depressions are often found in closely packed clusters of different sizes. Thus they may define areas with distinctive local geology. They can further be classified in two ways.

Two main groups can be identified by location: one group is related to the dichotomy boundary between the northern lowlands and southern highlands (L1) while the other occupies the western rim of Hellas (L2). Some sporadic samples can also be found, mainly in the highlands (L3) (Fig. 1).

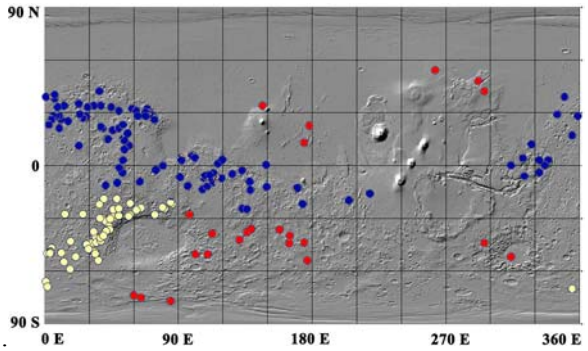

Figure 1. Map showing the positions of the craters found in the study. The dichotomy boundary craters (L1) are marked in dark blue, Hellas rim craters (L2) in light yellow. Sporadic craters (L3) are marked in red. At the time of writing this abstract, only areas between 0-180 E have been studied thoroughly.

Two additional categories are identified according to the shape and size of the collapse related to the crater. In roughly 1/3 of the samples the depressions are small and cover at maximum only half of the area of the crater floor (type S1). Their depressions are asymmetric, and don't appear to follow the crater shape very well (Fig. 2a).

Almost all other depressions are of the second type (S2, Fig. 2b). They form narrow streaks or cracks which run along the crater floor in a more symmetric way. Individual streaks can be identified to be either concentric or radial, and they usually cover almost the entire circumference of the crater floor in length. Looking at several craters, their evolution can be traced from single cracks up to chaotic-like terrain [7]. This type of depression is often clearly associated with fluvial processes.

On the eastern rim of Hellas, at same latitude as the L2 craters, there are several large outflow channels which indicate that there was water at the given latitude at some point in the planet's history, e.g. [1, 8, 9]. The water was probably originally in permafrost, which was afterwards released into liquid form by

nearby volcanic activity and geothermal heat. On the western rim of the basin [10], however, there are no volcanoes, and the permafrost in that area might have been trapped in the ground until a different method of release was found. The L2 craters are generally also of the type S1, without any runoff channels or other clear fluvial features. If they were created by volatile release, the collapses could be a result of water evaporation straight into the atmosphere. There might be underground channels beneath the surface, into which the ground water would have flowed - this could also indicate that some deep buried faults or grabens were among the processes involved in creating the depressions.

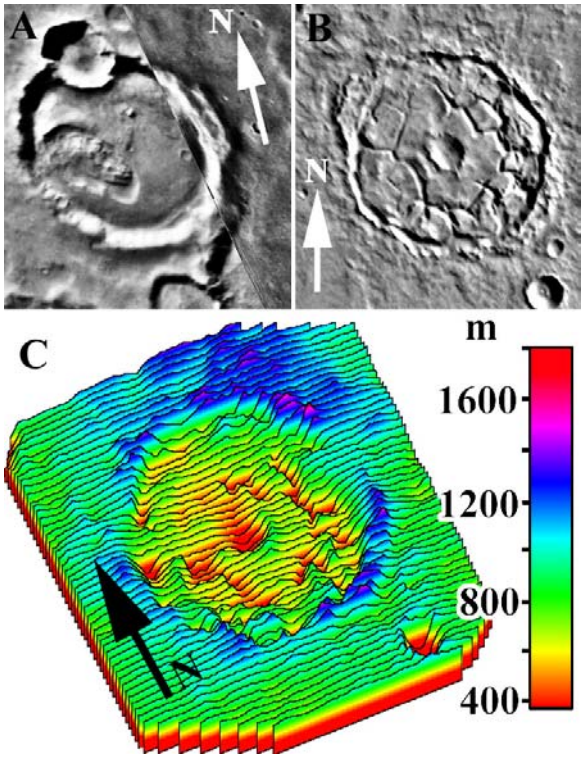

Figure 2. A) Depression type S1 example: non-concentric depression inside a crater. Image center: 50 S, 335.5 W. B) Type S2: narrow cracks around the crater floor, following the shape of the crater. Center of image is at 5 S, 252 W. C) Topographic representation of the S2 crater. The width of the craters is ~50 km.

Discussion: The inter-crater depressions are probably results of several different processes, all of which have removed material from within the crater floor. One such process is the deformation of the crust in larger scale or local faulting – e.g. graben formation and subsequent collapse of the surface material. It is also highly possible that volatiles were released from the ground either to the atmosphere or via fluvial channels, and resulted in cavity collapses. Hydrothermal systems can also play a part in the process. It is thus very likely that there was not only one but several processes affecting the formation of the depressions within the floor of impact craters locater in special Martian paleo-environments.

References: [1] Aittola, M. et al. (2002) *LPS XXXIII*, PDF #1485 (CD-ROM). [2] Kirk, R. L. et al. (2000) *LPS XXXI,* PDF #2011 (CD-ROM). [3] MOLA Team (1997) *http://ltpwww.gsfc.nasa.gov/Tharsis/mola.html.* [4] Caplinger, M. A. et al. (1999) *LPS XXX,* PDF #1659 (CD-ROM). [5] Bell, J. F. et al. (2003), *LPS XXXIV,* PDF #1993 (CD-ROM). [6] Fergason, R. L. and Christensen, P. R. (2003), *LPS XXXIV,* PDF #1785 (CD-ROM). [7] Newsom, H. E. (2001) *LPS XXXII,* PDF #1402 (CD-ROM). [8] Kostama, V.-P. et al. (2001) *Vernadsky-Brown*, abstract MS040. [9] Kostama, V.-P. et al. (2002) *LPS XXXIII*, PDF #1486 (CD-ROM). [10] Aittola, M. et al. (2001) *Vernadsky-Brown,* abstract MS002.

IMPACT LITHOLOGIES AND POST-IMPACT HYDROTHERMAL ALTERATION EXPOSED BY THE CHICXULUB SCIENTIFIC DRILLING PROJECT, YAXCOPOIL, MEXICO. David A. Kring[1], Lukas Zurcher[1], and Friedrich Horz[2], [1]Lunar and Planetary Laboratory, 1629 E. University Blvd., Tucson, Arizona USA 85721 (kring@LPL.arizona.edu), [2]NASA Johnson Space Center, NASA Road One, Houston, Texas USA 77058.

Introduction: The Chicxulub Scientific Drilling Project recovered a continuous core from the Yaxcopoil-1 (YAX-1) borehole, which is ~60-65 km from the center of the Chicxulub structure, ~15 km beyond the limit of the estimated ~50 km radius transient crater (excavation cavity), but within the rim of the estimated ~90 km radius final crater. Approximately ~100 m of melt-bearing impactites were recoverd from a depth of 794 to 895 m, above ~600 m of underlying megablocks of Cretaceous target sediments, before bottoming at 1511 m. Compared to lithologies at impact craters like the Ries, the YAX-1 impactite sequence is incredibly rich in impact melts of unusual textural variety and complexity. The impactite sequence has also been altered by hydrothermal activity that may have largely been produced by the impact event.

Impact Lithologies: The principal impact melt unit is a coherent 24-m thick green impact melt near the base of the impactite sequence. The melt is generally massive in appearance, but contains flow lines on both macroscopic and microscopic scales that are suggestive of glass; nevertheless, the melt is dominated by microcrystalline (2 to 50 μm) Ca-rich pyroxene ($Wo_{46-50}En_{41-35}Fs_{11-15}$), plagioclase ($An_{36-58}Ab_{60-40}Or_{2-9}$), and alkali feldspar ($An_{0-12}Ab_{98-9}Or_{2-90}$), which is similar to the melt recovered from the Yucatan-6 borehole ~50 km from the center of the crater [1-3]. The green melt is also brecciated and highly altered along its margins where the contacts were conduits for carbonate-rich fluids. A 10 m-thick carbonate-charged and brecciated green impact melt unit with large clasts of target material, including a 34 cm granite, was logged below the principal 24-m thick green melt unit. This may be the basal portion of the green melt unit or possibly a distinct melt unit.

A series of melt-rich breccias lie above the green melt unit and are composed of an unusual agglomerate of melt clasts, ranging from distinctly brittle melt fragments to flowed bodies. A 15 m-thick unit occurs immediately above the green melt unit and contains abundant and sometimes very large (up to 20 cm) clasts of banded melts. The melt is dominated by microcrystalline (<20 μm) pyroxene ($Wo_{46-51}En_{43-37}Fs_{10-13}$), plagioclase ($An_{48-56}Ab_{48-41}Or_{5-2}$), and alkali feldspar ($An_{0-9}Ab_{1-42}Or_{49-99}$), similar to the green melt although the colors of the banded melts are often different. These melts exist in a breccia that is variously clast and matrix supported, the latter of which appears to have been a conduit for post-impact fluids and is now charged with secondary alkali feldspar and carbonate.

A incredibly melt-rich, 23-m thick, breccia is next in the sequence. It is dominated (up to 82%) by fragments of altered silicate impact melt, generally with microcrystalline textures (<10 μm equant pyroxene, <50 μm long feldspar needles), although some fragments appear to have been partly to wholly glassy before being replaced by phyllosilicates and calcite. Primary minerals in the microcrystalline melts include pyroxene ($Wo_{48-51}En_{42-35}Fs_{10-14}$), plagioclase ($An_{50-59}Ab_{39-45}Or_{2-5}$), alkali feldspar ($An_{0-1}Ab_{0-10}Or_{100-88}$ and $An_5Ab_{94}Or_1$), magnetite, and Fe,Ti-oxides. Some of these silicate melts contained immiscible carbonate melt, gas vesicles (some of which were subsequently filled with secondary calcite and silicates), and flow-aligned crystals. Parts of the unit are clast supported, although the amount of matrix increases from ~15 to ~24% with depth. The matrix is composed of calcite, an altered silicate phase, and magnetite. The melt fragments have several different colors.

Above this unit is a 15 m-thick breccia unit with less melt. It is matrix-supported, with a variety of melt, sedimentary, and crystalline clasts up to 7 cm. Secondary carbonate permeates portions of the matrix and fills a 7 cm cavity. The uppermost impact unit is 13 m thick, a finer-grained version of the same material, and has been reworked, presumably by currents on the seafloor of the Gulf of Mexico, possibly induced by the impact. Secondary carbonate also permeates the matrix of this unit and forms a 2 cm-wide vein.

Excavated Components: The melts are dominated by silicate compositions, indicating they were excavated from the crystalline basement beneath the ~3 km-thick carbonate and evaporite platform sequence in the target area. Surviving clasts of crystalline materials include isolated quartz, feldspar, magnetite, and altered mafic minerals, and lithic clasts of granite-granodiorite, metaquartzite, shale, and unidentified mafics. Small amounts of immiscible carbonate melt in silicate melt fragments and clasts of micritic carbonate in the breccias indicate limestone was also excavated, some as melt. The siliceous and feldspathic lithologies are similar to those seen in the Yucatan-2, Yucatan-6, and Sacapuc-1 boreholes [1-5]. The mafic lithologies are new, although there were chemical and isotopic hints

of mafic target components in the Yucatan-6 core [3, 6]. Conspicuously missing in the melt-rich breccias are clasts of anhydrite (or even secondary anhydrite, both of which were present in Yucatan-2 and Yucatan-6 breccias [1,2]), possibly because of differentiation during the excavation, transportation, and/or deposition of target material.

Transport and Deposition: In general, material that lies outside the peak ring may have been ejected on ballistic paths that generated intense turbulent mixing or slid off the rising and then collapsing central uplift, perhaps to slosh back and forth between the rim of the crater and the peak ring. Collapse of large crustal blocks during the modification stage (and potentially later if there was additional settling) can also brecciate and rework deposits.

All the YAX-1 melts cooled quickly to form glassy to microcrystalline textures. Schlieren indicates melts were being mixed, but they were not mixed to the extent found in large central melt sheets. The melts solidified before the mixing process was complete, likely reflecting excavation from the transient crater and transport as small, discrete melt volumes. Minor amounts of melt encasing melt indicate some collisions and turbulence during transport. These streams of melt were fragmented after solidification, producing angular fragments or shards, although ribbony, fluidal fragments also survive.

In the case of the melt-rich breccias, the melt was shattered after it solidified and then mixed with carbonate-rich matrix components or was invaded by fluids precipitating secondary calcite. Because portions of the breccias are matrix supported, some carbonate had to be part of the original deposit, rather than having been introduced entirely by secondary fluid processes.

The 23 m-thick melt-rich breccia was deposited at temperatures too low (<1000 °C) for the melt fragments to be plastically deformed. Fragments of melt with gas vesicles and small once-glassy melt shards were not flattened, nor is there any indication of foliation as in a welded ash flow. Temperatures were also less than a few hundred degrees Celsius, because the carbonate-rich matrix did not form a carbonatite-like melt and micritic carbonate clasts in the carbonate-rich matrix were not resorbed.

The green melt was deposited and solidified as a coherent melt unit and was subsequently brecciated.

Fracturing: The entire impactite sequence was altered by post-impact hydrothermal processes, which were facilitated by high permeability throughout the core interval. A preliminary assessment of permeability was made by estimating fracture densities in color scans of the recovered core. Fracture densities range from 0 to 70%. With the exception of the interface between the upper two suevitic units (~808 m), which may have been reworked, the highest fracture densities occur near lithologic contacts. As noted above, these contact zones also exhibit the most prominent hydrothermal veining and brecciation.

Hydrothermal Alteration: From bottom to top, the impactite sequence exhibits increasingly more abundant Na for Ca exchange in primary feldspars and incipient scapolization. This Ca-Na alteration is crosscut by (biotite)-K feldspar-magnetite-calcite veins and extensive but diffuse K feldspar (adularia?) and magnetite replacement fronts.

From the bottom to the top, ilmenite is increasingly replaced by rutile. At the shallowest levels, both rutile and ilmenite are in turn replaced by sparse hydrothermal hematite. Iron-oxide barometry suggests that the oxidation state in the green melt unit at the bottom of the section is more reduced than the overlying breccias.

Potassium alteration is in turn followed by a calcite-chlorite-clay association. Chlorite appears to form after pyroxene and amphibole, and clay replaced chlorite. In addition to calcite, molybdenite and chalcopyrite are present in trace amounts in late calcite-clay veins and in vugs lined with barite.

The alteration sequence, plus stable isotope data [7], suggest a preexisting saline basinal brine was mobilized by impact heating. Calcium-Na and probably K metasomatism alteration probably occurred above 350 °C. However, K metasomatism could have been produced by downward percolation of cooler alkaline saline brines [i.e., 8]. Low temperature alteration assemblages containing calcite and phyllosilicates are also likely to be a product of post-impact hydrothermal activity, rather than diagenesis, because fluid inclusions in calcite suggest temperatures (>100 °C [9]) far in excess of normal temperatures at a depth of ~1 km.

References: [1] Kring D.A. et al. (1991) *LPS XXII*, 755-756. [2] Hildebrand A.R. et al. (1991) *Geology*, *19*, 867-871. [3] Kring D.A. and Boynton W.V. (1992) *Nature*, *358*, 141-144. [4] Sharpton et al. (1992) *Nature*, *359*, 819-821. [5] Sharpton et al. (1996) *GSA Sp. Paper*, *307*, 55-74. [6] Kettrup et al. (2000) *Meteoritics Planet. Sci.*, *35*, 1229-1238. [7] Zurcher L. et al. (2003) *LPS XXXIV*, Abstract #1728. [8] Johnson D.A. and Barton M.D. (2000) SEG GS 32, 145-162. [9] Luders V. et al. (2003) *LPS XXXIV*, Abstract #1378.

Acknowledgements: We thank the International Continental Drilling Program, Universidad Nacional Autonoma de Mexico, and the Chicxulub Scientific Drilling Project for producing the Yaxcopoil core. This work was supported by NSF grant EAR-0126055.

INFERRED PRIMARY COMPOSITIONS OF ARCHEAN SPHERULES FORMED BY THE CONDENSATION OF AN IMPACT-PRODUCED ROCK VAPOR CLOUD, BARBERTON GREENSTONE BELT, SOUTH AFRICA. A. E. Krull[1], D. R. Lowe[1] and G. R. Byerly[2], [1]Department of Geological and Environmental Science, Stanford University, Stanford, CA 94305-2115, [2]Department of Geology and Geophysics, Louisiana State University, Baton Rouge, LA 70803-4101.

Introduction: Based on the lunar cratering record, impacts were larger and more frequent on the early Earth than they are today. There is no persevered record of these early terrestrial impacts because rocks of this age have been obliterated by tectonism and erosion. The oldest known evidence of impacts on Earth lies in four beds (S1, S2, S3 and S4) in the Barberton Greenstone Belt (BGB), South Africa, ranging in age from about 3.24 to 3.47 Ga [1,2]. These beds are composed in large part of sand-sized spherical particles, termed spherules, that are thought to have formed by the condensation of rock vapor clouds ejected above the atmosphere as a result of large impacts [2]. Spherule beds S2 and S3 are both about 20 cm thick where composed entirely of fall-deposited spherules and up to a meter thick where spherules are mixed with locally derived debris. The diameters the bolides have been estimated to be between 20 and 50 km, based on bed thickness, size of the largest spherules, Ir fluence and extraterrestrial Cr [2,3,4].

The spherules range widely in size, composition, and texture within individual beds. Because of extensive diagenesis and metasomatism, they are now composed primarily of quartz, phyllosilicates, Ti-oxides and, in some cases, spinel. The main objective of this study is to estimate the original mineralogy of spherules in layer S3 through an analysis of preserved textures, compositions, and alteration products.

Spherule types: Preserved spherules represent 4 main compositional groups: (1) large, nearly pure silica spherules, commonly up to 4mm in diameter, (2) small phyllosilicate-rich spherules that range from 0.25 to 1mm in diameter and are often flattened, (3) compositionally layered spherules that are generally about 1-1.5mm in diameter and are composed predominantly of phyllosilicates with silica cores, although some have multiple phyllosilicate layers, and (4) mottled spherules composed of patchy silica and phyllosilicate with diameters between 1 and 2mm. A small percentage of spherules do not fall into these categories.

Mineralogy: Preserved primary mineral components in S3 include Ni-rich spinels [3] and detrital quartz and zircon. Rutile may also be primary, though it is more likely an alteration mineral. The low-temperature phase of TiO_2, anatase, is also present and these polymorphs may be the alteration products of one or more of the Ti-bearing minerals: pyroxene, titanite, perovskite, illmenite, and ulvospinel. Anatase is most common in the cores and around the rims of spherules, similar to the distribution of perovskite in CAIs [5]. Spinel also forms concentric layers within the centers of spherules and around spherule rims (Figs. A and B.) Where they occur in spherule cores, these early-formed minerals may have crystallized directly from a vapor and acted as nuclei for further condensates. Those along the outer margins of spherules more likely crystallized from melt droplets as it cooled forming rims. Rutile is common in altered komatiites and is derived from pyroxene and glass, and textural similarities between the two are currently under investigation.

Large silica spherules: The large silica spherules often display a sweeping undulatory extinction under cross-nicols, a feature characteristic of devitrification. These spherules also lack Al, Ti, Zr, Cr and other largely immobile elements. A small number of the large spherules show a faint relict barred texture characteristic of olivine and probably formed originally as a glass with a composition approaching that of olivine (Fig. C.) Fe and Mg have been regionally mobilized and removed during diagenesis/ metasomatism and accompanying silicification. This is consistent with a target rock composed largely of basalt and komatiite and a chondritic bolide, as suggested by Byerly and Lowe [3].

Phyllosilicate-rich spherules: The phyllosilicate-rich spherules commonly show a relict fibroradial texture (Fig. D) radiating inward from the outer margin. Many have a spherical mass of cavity-fill quartz at or near the center. These spherules have cooled rapidly inward from the outer margin towards the centers of the droplets, with trapped unexolved gas at the cores. The central vacuoles have since been filled with coarse quartz. In chondrules, quenched pyroxene has a similar fibroradial texture [6]. Because the relict fibroradial crystalites contain abundant Al, the precursor must also have been Al-rich. Additionally, the spherules with this texture contain dispersed TiO_2 (Fig. E.) Therefore they cannot represent olivine. Fassaite, an Al-Ti-rich pyroxene, is commonly seen in CAIs [7] and may have crystallized in the spherules as well. Alternatively, komatiitic-tholeittic augite in the BGB contain abundant Al_2O_3 and TiO_2. These would not require direct crystal-vapor condensation, and therefore augite may be a more likely precursor. Plagioclase could also crystallize with a similar quench texture [8] but because of the

abundance of TiO_2 and because the target rock was probably basaltic, pyroxene is more likely.

Although compositionally similar, a distinct population of smaller phyllosilicate-rich spherules do not display relict textures, and their original mineralogy is unknown. At least three different phyllosilicates are present in the spherules and further analyses are required. The spherules appear to have rigid outer margins and more ductile interiors, as some are broken with the interior material squeezed out (Fig. F.) Lowe et al. [9] have suggested that spherule deformation occurred during diagenesis.

Layered spherules: Layered spherules may have formed by a variety of mechanisms: (1) Small spherules crystallized and acted as nuclei for later condensation of material from the vapor cloud. (2) Droplets of different viscosities collided in the turbulent atmosphere and vapor cloud, and the less viscous droplet enveloped the more viscous droplet. This formation mechanism is suggested by common differences in sphericity of the layers within individual spherules. The inner layer is almost always more spherical than the spherule as a whole, suggesting the early-formed spherule was already rigid when the outer layer formed. Also, some spherules show a dumbbell shape reflecting the incomplete merging of partially molten droplets following collision. (3) Some spherules may have formed with internal spherical cavities, similar to the fibroradial spherules discussed above, that were later filled. These spherules tend to have larger blocky quartz in the cores. All of these mechanisms are thought to have formed spherules in S3.

Conclusions: Spherule bed S3 shows a variety of spherule types. Some of the original mineralogy can be inferred from relict textures and alteration products. Primary minerals included Ni-rich spinels, olivine, pyroxene and possibly plagioclase. Anatase and rutile are found in the cores and rims of spherules and likely represent alteration from pyroxene and possibly some other high temperature Ti-oxides. A more thorough understanding of the mineralogy will offer important constraints on the condensation processes of rock vapor clouds produced by large impacts.

Work in progress. We are currently developing a mixing model to determine the composition of the target rock and the ratio of target rock to bolide in the rock vapor cloud. The bolide is inferred to have been a carbonaceous chondrite based on Cr isotopes [4,10]. This model will allow us to use the bulk composition to constrain the original mineralogy and glass compositions of spherules that condensed from the rock vapor cloud.

References: [1] Lowe, D.R. et al. (1989) *Science, 245,* 959-962. [2] Lowe, D.R. and Byerly, G.R. (1986) *Geology, 14,* 83-86. [3] Byerly, G.R. and Lowe, D.R. (1994) *GCA, 58*, 3469-3486. [4] Shukolyukov, A. et al. (2000). *Impacts and the Early Earth,* 99-115. [5] Brearly and Jones (1998) *Reviews in Mineralogy, 36*, Ch.3. [6] Nagahara, H. (1983) *Mem. Natl. Inst. Polar Res. Sp. Issue 30,* 61-83. [7] Marvin et al. (1970) *EPSL, 4,* 346. [8] Simonson et al. (2000) Aust. J. of Earth Sci., 47, 315-325. [9] Lowe, D.R. et al. (2003) *Astrobiology, 3,* 7-48. [10] Kyte et al. (2003) Geology, 31, 283-286.

Acknowledgements: This research was supported by grants NCC2-721 and NAG5-9842 from the NASA Exobiology Program to DRL, the NSF Grant EAR-9909684 to GRB, and McGee Grants to AEK. We are thankful for the generous student travel support provided by The Barringer Crater Company to AEK. We are grateful to Anglovaal, ETC, and the AngloAmerican Mining companies for access to spherule bed samples.

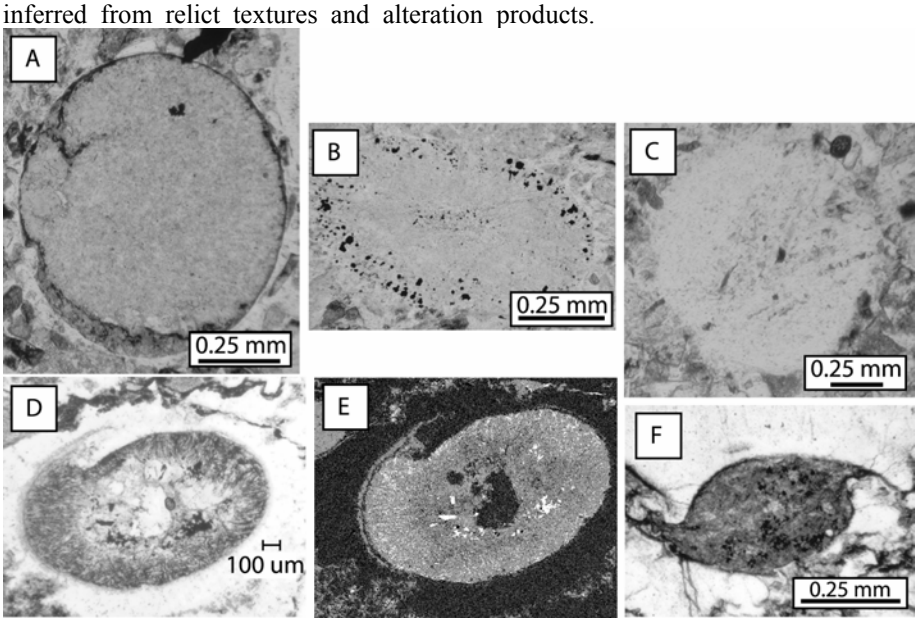

Figure: Examples of spherules seen in the S3 spherule bed. (A) A large spherule with a dark, fine-grained TiO_2 rim. (B) Spherule with Ni-rich spinel along rim and in the core of the spherule. (C) Faint ghost of barred olivine in a large silica spherule. (D) Spherule with fibroradial texture and originally hollow, now quartz filled center. (E) BSE photo of spherule in D. Bright spots are TiO_2. The rest of the spherule is composed of phyllosilicates and the dark areas are quartz. Note the dispersed anatase following the fibroradial texture. (F) Small deformed phyllosilicate spherule showing the stiff shell of the spherule and more ductile interior.

COMPARISON OF DISTAL IMPACT SPHERULES FROM KT BOUNDARY AND LATE EOCENE DEPOSITS. Frank T. Kyte, Center for Astrobiology, Institute of Geophysics and Planetary Physics, University of California, Los Angeles, CA 90095-1567, USA (kyte@igpp.ucla.edu).

Distal impact spherules provide information about impact processes that cannot be perceived by analyses of impact craters or numerical models. Two rather well-studied impact spherule deposits which are also relatively well preserved are the KT boundary and the late Eocene deposit containing clinopyroxene-bearing (cpx) spherules. The KT boundary spherules are almost certainly directly related to the Chicxulub impact event, and the late Eocene cpx spherule deposit is commonly believed to be derived from the Popigai event. These are the two largest impact structures in the last 100 Ma. These deposits have several common features, which may reflect processes common to large-body impacts as well as significant differences. I will concentrate on data from the KT boundary at DSDP Site 577, western N. Pacific and Eocene ejecta from ODP Site 709, western Indian Ocean.

The KT boundary is known to have at least two distinct spherule deposits [e.g., 1]. Large glass spherules are found beneath impact wave deposits of the Gulf of Mexico and are commonly attributed to impact melt from low-velocity ejecta that has a very low extraterrestrial component (i.e., low Ir content). These are probably distributed regionally, and not globally. They form the lower layer of the KT boundary couplet in the Western Interior, N. America and traces of large, hollow spherules found in N. Pacific sites GPC3 and DSDP 577 may also be from this source. The Ir-rich global fallout is also composed mostly of spherules. It's origin is probably largely from the impact plume [2], but may also contain materials derived directly from meteoritic materials [3]. The KT boundary is known at well over 100 sites; the mean amount of Ir deposited is on the order of 55 ng/cm^2 [4].

The KT boundary at DSDP 577 probably has the best preserved spherules of any site. However, in nearly all cases, most of the silicates have been replaced by clay minerals, so bulk chemical analyses of the original major element chemistry are impossible. The high degree of preservation is probably related to shallow burial at Site 577 (109 m) and oxidizing, rather than reducing conditions following burial. Three high-temperature minerals have been identified at this site. Clinopyroxene (cpx), found only at Site 577 may be the precursor to diagenetic sanidine in some European sites [5]. Magnesioferrite spinel [6] has the highest Fe_2O_3/FeO of any KT locality [2] and can have trace inclusions of Ni-rich magnesiowustite [7], which is known at only one other site (Site 596, S. Pacific). Other debris described includes shocked quartz grains >200 μm [8], hollow spherules possibly related to regional glass deposits [1,5], and irregular Ir-rich particles that may be unmelted meteoritic materials [9]. The latter may be related to the fossil meteorite found at DSDP Site 576, just 500 km to the east [10].

A large-volume (~10 cc) sample from DSDP 577 provided a 44 mg carbonate-free residue (>60 μm) composed nearly entirely of impact debris. Nearly 2700 particles >100 μm were classificatied based on color, shape, and morphology. Although they form a rather complex assemblage of spherules and other particles, they gan be generally described as ~60% light colored spherules and ~40% dark colored spherules. The light-colored spherules are mostly white, but can contain dark inclusions, and several percent of the total include green, cpx-bearing spherules and fragments of large, hollow spherules.These have generally low siderophile element concentrations (Fe, Cr, Ni, Co, Ir) and are probably derived from a target-rich portion of the impact plume. Many were found to have pseudomorphic textures similar to the dendritic textures of cpx spherules, so it's likely that many, if not all of these are altered from hi-Ca pyroxene (±glass?). The dark colored particles have a broad range of siderophile element concentrations, but are generally more enriched in the meteoritic component than the light spherules. As noted by [3] some of these particles have Ir concentrations comparable to those found in chondritic meteorites. The dark particles invariably contain magnesioferrite spinels, but the spinel content is quite variable, ranging from trace concentrations to perhaps 50% by volume of some spherules. A small fraction with high Ir have irregular outlines, and no obvious melt textures; these are the possible unmelted meteorite particles described by Robin et al. [3]. Hypotheses for origin of the spinel bearing spherules include origin in the projectile-rich portion of the impact plume [2] or as a form of ablation debris derived directly from meteoritic material [3]. Possibly, both are important sources of these particles. We have found several light-colored spherules with dark inclusions that are a mixture of the two main spherule types, with one or more inclusions of spinel-bearing material. We believe that this indicates that both types of material were coexisted as liquids, strongly supporting a plume origin for at least some fraction of the spinel-bearing spherules.

The late Eocene cpx spherule deposits contain a similar mix of particles to those in the KT boundary. They are much better preserved, commonly containing glass and unaltered cpx, so it is possible to determine bulk major element chemistry of the precursor materials. As with the KT boundary, there are two distinct components, a glassy microtektite that may be equivalent to the impact melt glasses of regional KT

deposits, and the cpx spherules that are distributed globally [11,12]. Isotopic analyses of these components have shown that the microtektites and cpx spherules are from the same source [13] and this is consistent with the Popogai crater [14]. Ir analyses have been reported for 12 sites and the mean Ir deposited in the late Eocene was on the order of 9 ng/cm^2, or about 16% of the KT value [15].

A large-volume sample from ODP Site 709 has yielded more than 17,000 cpx spherules, and several hundred microtektites (>125 μm), as well as shocked quartz and coesite [16]. The microtektites have a very low siderophile content (<100 pg/g Ir), while a bulk sample of the cpx spherules has ~1 ng/g (analyses in progress). As with the KT boundary, there are both light and dark-colored cpx spherules. Microprobe analyses of these spherules indicate that the main difference is that the light spherules have generally high CaO (12% vs. 6%, on average) and lower FeO (3.6% vs. 7.5%), and probably also lower Cr (but Cr data are near detection limits and imprecise). In general, this is consistent with a model in which the cpx spherules are from the impact plume, with the darker spherules from the more projectile-rich portion of the plume. Unlike the KT boundary spherules, spinels are never more than a trace phase in the cpx spherules, but they are clearly more common in the darker spherules.

Compared to the KT boundary, a significant component appears to be missing in the late Eocene deposits [15]. The coarse fraction of KT deposits holds the majority of the Ir and other siderophiles in well preserved deposits like DSDP 577. But in the Eocene sediments, the Ir in the cpx spherules can only account for a small fraction, at most a few per cent of Ir in the bulk sediment. Whether the principal Ir carrier is an ejecta component in the fine fraction, or some larger Ir component that is not preserved in sediments has yet to be determined.

Reference: [1] Smit J. (1999) Ann. Rev. Earth Plan. Sci. 27, 75. [2] Kyte and Bostwick (1995) EPSL 132, 113. [3] Robin et al. (1993) Nature 363, 615. [4] Donaldson S. and Hildebrand A.R. (2001) MAPS 36, A50. [5] Smit J. et al. (1992) Proc. LPSC 22, 87. [6] Smit J. and Kyte F.T. (1984) Nature 310, 403. [7] Kyte F.T. and Bohor B.H. (1995) Geochim. Cosmochim. Acta 59, 4967. [8] Bostwick J.A. and Kyte F.T. (1996) GSA. Spec. Pap. 307, 403. [9] Robin, E. et al. (1993) Nature, 363, 615. [10] Kyte F.T. (1998) Nature 396, 237. [11] Vonhof H.B. and Smit J. (1999) MAPS 34, 747. [12] Glass B.P. and Koeberl C. (1999) MAPS 34, 197. [13] Liu et al. (2001) LPSC XXXII, abs. 1819. [14] Whitehead J. et al. (2000) EPSL 181, 473 [15] Kyte F.T. and Liu S. (2002) LPSC XXXIII, abs. 1981. [16] Liu et al. (2002) MAPS 37, A88.

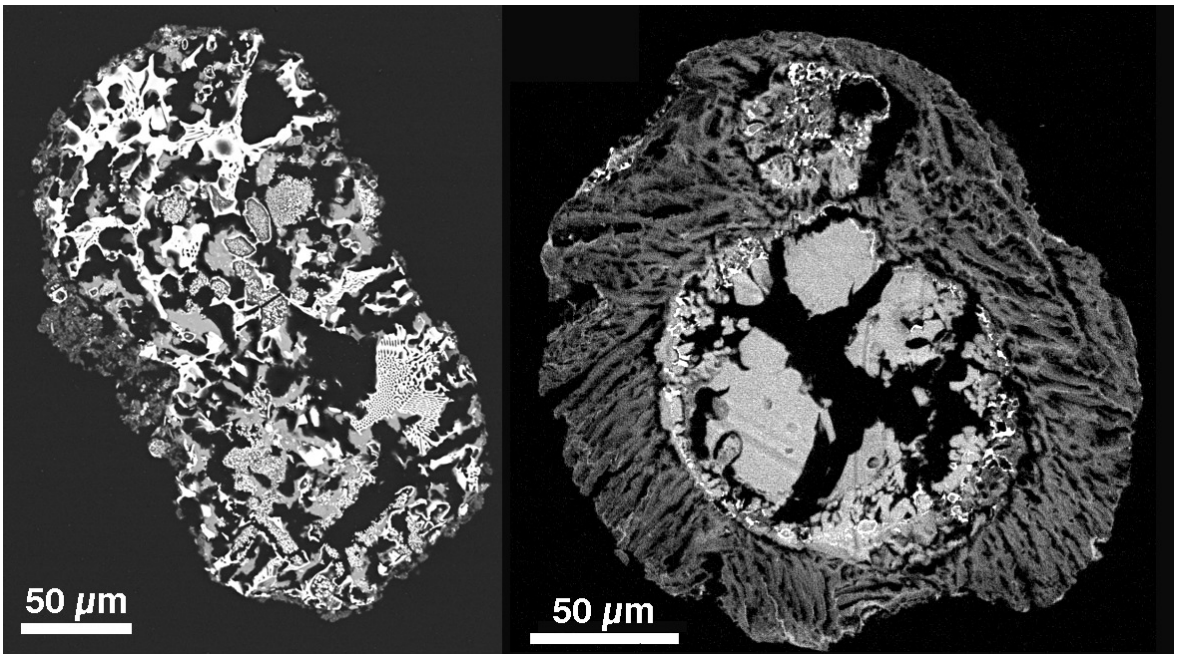

Figure. BSE images of polished sections of two KT boundary impact spherules. **Left**: very spinel-rich spherule. Nearly all the bright phases are anhedral, commonly porous, spinel. It's difficult to estimate the original proportion of spinel vs. silicates. During drying, clays shrink and separate. Dark voids are epoxy that has intruded the spherule during mounting. This spherule was probably at least 50% spinel by volume. **Right**: This is a typical light colored spherule, without spinel, that has inclusions of spinel-bearing material. Clearly these two components were both liquid at about the same time. They probably mixed together inside the impact plume.